DNA polymerase theta-mediated DNA repair is a functional dependency and therapeutic vulnerability in DNMT3A deficient leukemia cells.

Bac Viet Le[1], Umeshkumar Vekariya[1], Monika M. Toma[1], Margaret Nieborowska-Skorska[1], Marie-Christine Caron[2], Malgorzata Gozdecka[3], Zayd Haydar[1], Martin Walsh[4], Jayashri Ghosh[1], Elaine Vaughan-Williams[1], Paulina Podszywalow-Bartnicka[5], Anna-Mariya Kukuyan[1], Sylwia Ziolkowska[1], Emir Hadzijusufovic[6,7], Gurushankar Chandramouly[8], Katarzyna Piwocka[5], Richard Pomerantz[8], George S. Vassiliou[3], Brian J.P. Huntly[3], Peter Valent[9,10], Alfonso Bellacosa[4], Jean-Yves Masson[2], Gaorav P. Gupta[11], Grant A. Challen[12], Tomasz Skorski[1,13,14*]

[1]Fels Cancer Institute for Personalized Medicine, Lewis Katz School of Medicine, Temple University, Philadelphia, PA 19140, USA

[2]CHU de Québec Research Centre (Oncology Division) and Laval University Cancer Research Center, Québec City, QC, Canada.

[3]Wellcome-MRC Cambridge Stem Cell Institute, University of Cambridge, Cambridge, United Kingdom.

[4]Cancer Epigenetics Institute, Fox Chase Cancer Center, Philadelphia, Pennsylvania; Nuclear Dynamics and Cancer Program, Institute for Cancer Research, Fox Chase Cancer Center, Philadelphia, PA, USA

[5]Laboratory of Cytometry, Nencki Institute of Experimental Biology Polish Academy of Sciences, 02-093 Warsaw, Poland.

[6]Ludwig Boltzmann Institute for Hematology and Oncology and Department of Internal Medicine I, Division of Hematology and Hemostaseology, Medical University of Vienna, Vienna, Austria.
[7]Department for Companion Animals & Horses, Clinic for Internal Medicine and Infectious Diseases, University of Veterinary Medicine Vienna, Vienna, Austria.

[8]Department of Biochemistry and Molecular Biology, Sidney Kimmel Cancer Center, Thomas Jefferson University, Philadelphia, PA, USA

[9]Department of Internal Medicine I, Division of Hematology and Hemostaseology, Medical University of Vienna, Vienna, Austria

[10]Ludwig Boltzmann Institute for Hematology and Oncology, Medical University of Vienna, Vienna, Austria

[11]Lineberger Comprehensive Cancer Center, University of North Carolina at Chapel Hill, Chapel Hill, NC, USA

[12]Division of Oncology, Department of Medicine, Washington University School of Medicine, Saint Louis, MO, USA

[13]Department of Cancer and Cellular Biology, Lewis Katz School of Medicine, Temple University, Philadelphia, PA, USA

[14]Nuclear Dynamics and Cancer Program, Fox Chase Cancer Center, Philadelphia, PA, USA

[*]Corresponding Author:

Tomasz Skorski - Fels Cancer Institute for Personalized Medicine, Lewis Katz School of Medicine, Temple University, Philadelphia, PA 19140, USA. Email: tskorski@temple.edu

Conflict of Interest.

G.A.C. has performed consulting and received research funding from Incyte, Ajax Therapeutics and ReNAgade Therapeutics Management, and is a co-founder, member of the scientific advisory board, and shareholder of Pairidex, Inc. RTP is a co-founder and chief scientific officer of Recombination Therapeutics, LLC. Other Authors declare no conflict of interest.

Abstract

Myeloid malignancies carrying somatic *DNMT3A* mutations (*DNMT3Amut*) are usually resistant to standard therapy. *DNMT3Amut* leukemia cells accumulate toxic DNA double strand breaks (DSBs) and collapsed replication forks, rendering them dependent on DNA damage response (DDR). DNA polymerase theta (Polθ), a key element in Polθ-mediated DNA end-joining (TMEJ), is essential for survival and proliferation of *DNMT3Amut* leukemia cells. Polθ is overexpressed in *DNMT3Amut* leukemia cells due to abrogation of PARP1 PARylation-dependent UBE2O E3 ligase-mediated ubiquitination and proteasomal degradation of Polθ. In addition, PARP1-mediated recruitment of the SMARCAD1-MSH2/MSH3 repressive complex to DSBs was diminished in *DNMT3Amut* leukemia cells which facilitated loading of Polθ on DNA damage and promoting TMEJ and replication fork restart. Polθ inhibitors enhanced the anti-leukemic effects of mainstream drugs such as FLT3 kinase inhibitor quizartinib, cytarabine and etoposide in vitro and in mice with FLT3(ITD);*DNMT3Amut* leukemia. Altogether, Polθ is an attractive target in *DNMT3Amut* hematological malignancies.

Introduction

DNA (cytosine-5)-methyltransferase 3A (DNMT3A) loss of function either by somatic mutation, allelic loss and epigenetic-dependent abrogation of expression has been found in solid tumors (e.g., lung and colon cancers, melanoma) and in hematological malignancies such as acute myeloid leukemia (AML), myeloproliferative neoplasm (MPN) and chronic myeloid leukemia (CML) blast phase (1-4). DNMT3A adds a methyl group to the cytosine residue in DNA, generating 5-methylcytosine (5-mC) (5). Somatic *DNMT3A* mutations lead to a loss of protein function and are associated with resistance to standard treatments such as anthracyclines (including daunorubicin, the component of standard "7+3" induction chemotherapy for AML), interferon alpha (IFNα), BCL-2 inhibitor venetoclax, and ABL1 tyrosine kinase inhibitor imatinib (6-9), resulting in unfavorable outcomes and adverse prognosis (7,8,10-13). Also, *DNMT3A*-mutated clones are commonly detected during remission, likely contributing to disease relapse (7,14). Altogether, these observations suggest that malignant clones carrying *DNMT3A* mutations are difficult to eliminate. Thus, novel therapeutic strategies against *DNMT3A* mutated hematological malignancies need to be developed.

AML, MPN and CML cells expressing oncogenic tyrosine kinases (OTKs) such as FLT3(ITD), JAK2(V617F), MPL(W515L) and BCR-ABL1 accumulate spontaneous DNA damage, including highly toxic DNA double strand breaks (DSBs), induced by metabolic products and replication stress (15-18). To repair abundant DSBs and protect the cells from pro-apoptotic effect of DSBs, leukemia cells might activate the DNA damage response (DDR) involving the pathways sensing DSBs (ATM and ATR kinases), repairing DSBs (RAD51-mediated homologous recombination = HR, RAD52-mediated transcription associated homologous recombination = TA-HR and single strand annealing = SSA, DNA-PK -mediated non-homologous end-joining = NHEJ, Polθ-mediated end-joining = TMEJ) as well as these

activating checkpoints to arrest cell cycle (via CHK1 and CHK2 kinases) (19,20). In addition, PARP1 is required in various aspects of DDR (21).

We reported that somatic mutations in *TET2* (ten-eleven translocation 2) caused HR and NHEJ deficiencies resulting in sensitivity of AML/MPN/CML cells to PARP1 inhibition; conversely, leukemia cells carrying *DNMT3A* mutations were resistant (22). Here we show that DNA polymerase theta (Polθ), a key element in TMEJ, is essential for survival of AML/MPN/CML cells carrying *DNMT3A* mutations, but not these with *TET2* mutations.

Polθ, encoded by *POLQ* gene, is a large protein (290 kDa), and includes an amino-terminal helicase domain and a carboxy-terminal polymerase domain (23). Polθ helicase domain captures of two ssDNA strands with microhomologies, bringing them in close proximity (24). Then, Polθ polymerase domain binds to forms a synaptic complex and initiate repair synthesis. In addition to playing a key role in TMEJ, Polθ also works in restarting stalled replication forks and in ssDNA gap filling (25-29). Polθ is emerging as a therapeutic target in cancer because of the synthetic lethal effect of inhibition of Polθ in HR-deficient tumors (23).

Although DNMT3A deficiency did not cause detectable changes in HR in tumor cells (22,30), we show that these cells are highly sensitive to pharmacological and genetic inactivation of Polθ. Remarkably, we discovered that DNMT3A inactivation promoted Polθ overexpression due to inhibition of PARP1-mediated PARylation-dependent ubiquitination (PARdU) of Polθ by UBE2O E3 ligase resulting in reduced proteasomal degradation of Polθ. DNMT3A-deficient leukemia cells displayed increased loading of Polθ on DNA damage, limited end resection, and enhanced TMEJ and replication fork restart. We also demonstrated that Polθ inhibitors combined with standard drugs could be used to eradicate *DNMT3A*-mutated malignant clones, which are resistant to most of current therapeutics.

Materials and Methods

Primary human leukemia cells and cell lines

Lin-CD34+ AML patient cells (n=3 of each) carrying FLT3(ITD), and FLT3(ITD) accompanied by *TET2mut* or *DNMT3Amut* were characterized before (22). $Lin^{-}CD34^{+}$ cells were obtained from mononuclear fractions by magnetic sorting using the EasySep Lin negative selection followed by CD34 positive selection cocktail as described before (31). Human AML primary cells were incubated in StemSpan®SFEM medium (Stem Cell Technologies, Vancouver, Canada) supplemented with the cocktail of growth factors (100 ng/ml SCF, 20 ng/ml IL-3, 100 ng/ml FLT-3 ligand, 20 ng/ml G-CSF, 20 ng/ml IL-6) as described before (31). JAK2(V617F)-positive human HEL cells and JAK2(V617F);*DNMT3A*(R882H)-positive human SET-2 cells were described before (32,33).

Primary murine cells and cell lines

$Lin^{-}cKit^{+}$ murine bone marrow cells were obtained from the following genetically modified mice: (1) $Flt3^{ITD}$, $Flt3^{ITD}$;$Tet2^{-/-}$ and $Flt3^{ITD}$;$Dnmt3a^{-/-}$, and $FLT3^{ITD}$;$Parp1^{-/-}$ which were described before (18,22); (2) *Vav-Cre(+);*$Dnmt3a^{(f/f)}$;$Polq^{-/-}$ were generated by crossing *Vav-Cre(+);Dnmt3a(f/f)* and $Polq^{-/-}$, mice, and (3) *Mx-1-Cre;*$Dnmt3a^{R882H/+}$;$Flt3^{ITD/+}$ mice were generated by crossing $Dnmt3a^{floxR882H/+}$ mouse model (https://doi.org/10.1182/blood.V126.23.2424.2424) with *Flt3-ITD* (34) and *Mx1-Cre* mice (35). Cre expression was induced by intraperitoneal injection of 5- to 6-week-old mice with pIpC (Sigma P1530, 20mg/kg; five doses over a period of 10 days). Mouse ear snips were lysed with DirectPCR Lysis Reagent (Viagen, 401-E) according to the manufacturer's instructions. Lysed DNA was used for genotyping of each allele with the following primers:

Allele Name	Primer Name	Primer sequence 5' → 3'	Mutant Band	WT Band
Mx1-Cre	MxCre_1	GCGGTCTGGCAGTAAAAACTATC	~100bp	~300bp
	MxCre_2	GTGAAACAGCATTGCTGTCACTT		
	MxCre_3	CTAGGCCACAGAATTGAAAGATCT		

	MxCre_4	GTAGGTGGAAATTCTAGCATCATCC		
FLT3	FLT3_Fwd1	AGGTACGAGAGTCAGCTGCAGATG	~250bp	~200bp
	FLT3_Rev1	TGTAAAGATGGAGTAAGTGCGGGT		
Dnmt3a-R882H/+	hEx23_Rev1	GAGACGTCTGTGTAGTGGACG	~708bp	~600bp
	Dnmt3a5-F1	CCTGCACTTTTCTGTAGCTGG		
Dnmt3a-R882H/+ POST-CRE	Dnmt3a5-F1	CCTGCACTTTTCTGTAGCTGG	~300bp (recombined)	
	Enr2	GGGCAAGAACATAAAGTGACC		

PCR was performed with REDTaq ReadyMix PCR Reaction Mix (Sigma, R2523) with following conditions: initial denaturation at 95°C for 1 minute, followed by 35 cycles of 95 °C for 15 s, annealing at 57°C for 15s and elongation at 72°C for 15s. Final elongation was performed at 72°C for 10 minutes. PCR products were visualized on the 2.5% agarose gel (Supplemental Figure S1). Mice with proper genotypes were aged and sacrificed at signs of disease. $Lin^{-}cKit^{+}$ cells were obtained from mononuclear fractions by magnetic sorting using the EasySep Lin negative selection followed by cKit positive selection cocktail as described before (31). Murine normal and malignant hematopoietic cells were maintained in StemSpan®SFEM medium supplemented with: (normal cells, and CML-like and AML-like: 100 ng/ml SCF, 20 ng/ml IL-3 and IL-6; MPN-like: 100 ng/ml SCF; 10 ng/ml FLT3 ligand; 20 ng/ml IL-3, IL-6, G-CSF and GM-CSF; 12 units/ml EPO; 2.5 ng/ml TPO] as described before (16,31,36). FLT3(ITD) (F), FLT3(ITD);*Tet2-KD* (FT-KD) and FLT3(ITD);*Dnmt3a-KD* (FD-KD) 32Dcl3 cells were characterized before (22).

Expression constructs

pMIGR1-GFP was purchased from Addgene (cat# 27490). pMIG1-FLT3(ITD)-GFP, pMIG1-BCR-ABL1-GFP and pMIG1-JAK2(V617F)-GPF were described before (36). pCDH-EF1-FHC-POLQ (*POLQ*-wildtype) (#64875) and pCDH-EF1-FHC-POLQ-DY2230AA (*POLQ*-polymerase mutant) (#64878) were purchased from Addgene. *POLQ*-wildtype and *POLQ* polymerase mutant cDNAs were cloned into pCMMP-MCS-IRES-mRFP (Addgene #36972) by Fast Digest *BamH*I (#FD0054), *Not*I (#FD0596) and *Bgl*II (#FD0084) from ThermoFisher Scientific. In this

experiment, after enzymatic digestion, DNA fragments were purified by GeneJET Gel Extraction Kit (ThermoFisher Scientific #K0691) and then ligated by Rapid DNA Ligation Kit (ThermoFisher Scientific # K1422). Ligation products were then heat-shock transformed into *E. coli* DH5α. Single bacterial colony which survived in ampicillin agar LB medium was picked up for DNA plasmid extraction by Macherey-Nagel NucleoSpin Plasmid (#74049950). To confirm the sequence of *POLQ*-wildtype and *POLQ*-polymerase mutant, pCMMP-MCS-IRES-mRFP-POLQ and pCMMP-MCS-IRES-mRFP-POLQ-DY2230AA were sequenced by Sanger sequencing.

Viral infection

10 µg of the expression plasmid and 5 µg pCL-Eco (Addgene plasmid #12371) were co-transfected into Pheonix-Eco cells in the culture medium without antibiotics, to produce the retrovirus packaging these plasmids by Lipofectamin 2000 Transfection Reagent (ThermoFisher Scientific # 11668019). After 24 and 48 hours of the transfection, the retroviral production was obtained and purified by 0.45 µm pore filter. Next, 0.5 x 10^6 cells were suspended in 1 mL retroviral production, supplemented with 8 µg polybrene. The spin (540 g) infection was performed in 90 minutes at 30^oC, and the retroviral production was replaced by regular culture medium after 4 hours. GFP^+ and RFP^+ cell populations were obtained by flow cytometry. To produce the lentiviral production for the infection, 10 µg expression plasmid, 7 µg psPAX2 (Addgene cat# 12260), and 5 µg pMD2.G (Addgene #12259) were co-transfected into HEK 293T/17 cells (ATCC # CRL-11268) in the culture medium without antibiotics. The medium was refreshed every 24 hours. The lentiviral production was collected and purified by 0.45 µm pore-size filter after 24 and 48 hours. The spin infection was performed by resuspending 0.5 x 10^6 cells in 1 mL lentiviral production with 8 µg polybrene supplement, followed by the spin at 2200 rpm/30°C in 60 minutes. After the incubation at 37°C/5% CO_2 in 4 hours, the lentiviral production was replaced by regular medium. After 48 hours, GFP^+ cells were sorted by flow cytometry.

Knockdown of MSH2 and UBE2O

Cells were transfected with 2 μM shRNA of MSH2 (Dharmacon, cat# V3SM11241-234501644) or 200 nM siRNA-smart pool UBE2O [Dharmacon, cat# L-064151-01-0020, (J-064151-09, J-0654151-10, J-065151-11, J-064151-12)] co-transfected with 100 ng pCMMP-MCS-IRES-mRFP using Nucleofector™ kit (cat#. VPA-1003, Lonza, Germany). GFP^+ (MSH2 Knockdown) or RFP^+ (UBE2O knockdown) cells were sorted 48 hours post-transfection; downregulation of MSH2 or UBE2O was confirmed by Western blot.

Leukemogenesis in mice

Female SCID (C.B-17/IcrHsd-*Prkdc*^{scid}) mice were purchased from Inotiv (formerly Envigo #182). The animals were sub-lethally total body irradiated (2 Gy) and injected i.v. with (1) 1 x 10^6 GFP^+ Lin^-cKit^+ GFP^+ *Dnmt3a-/-* and *Dnmt3a-/-;Polq-/-* murine bone marrow cells (mBMCs) expressing FLT3(ITD), and (2) 1 x 10^3 RFP^+ FLT3(ITD);*Dnmt3a*-ko 32Dcl3 cells transduced with *POLQ* wild-type and DY2230AA dominant-negative mutant. GFP^+ and RFP^+ cells were detected in PBL by flow cytometry. Survival of the mice injected with 32Dcl3 cells was monitored.

Inhibitors and cytotoxic drugs

The following DNA repair inhibitors were applied: PARPi olaparib (Selleckchem, cat# S1060), ATMi KU60019 (EMD Millipore, cat# 531978), ATRi VE-821 (Selleckchem, cat# S8007), DNA-PKi II (EMD Millipore, cat# 260961), RAD52i DI-03 (37), RAD51i RI-1 (Selleckchem, cat# S8077), CHK1i rabusetib: (Selleckchem, cat# S2626), CHK2i BML-277 (Selleckchem, cat# S8632), Polθi novobiocin (Selleckchem, cat# S2492), Polθi ART558 (MedChemExpress, cat# HY-141520), Polθi ART812 (MedChemExpress, cat# HY-139289), and Polθi RP-6685 (MedChemExpress, cat# HY-151462). Polθi RTx-161 was synthesized as described (38). Etoposide (cat# S1225), cytarabine (cat# U-19920A), azacytidine (cat# S1782), C-176 (cat# S6575), PLK1i volasertib (cat# S2235), FLT3i quizartinib (cat# S1526) were purchased from

Selleckchem. DNMT3A selective inhibitor DNMT3A-IN-1 (cat# HY-144433) was from MedChemExpress (39). MG132 (cat# M7449), and hydroxyurea (cat# H-8627) were from Sigma. All compounds were dissolved, aliquoted and stored following manufacturer's instructions. Compounds were added for 1-3 days, as indicated, following by trypan blue exclusion viability test and/or plating in Methocult (Stemcell Technologies cat# 04320) when indicated; colonies were scored after 5-7 days.

Detection of proteins in total and nuclear cell lysates and in chromatin fractions

Nuclear and total cell lysates were obtained as described before (40). Chromatin bound proteins were isolated using a chromatin extraction kit (Abcam cat# ab117152) according to the manufacturer's instructions. Briefly, 1 x 10^7 cells were washed 2 times with PBS, followed by addition of 1x lysis buffer (1 x 10^6 cells/100 µL) containing protease inhibitor cocktail and incubated on ice for 10 min. The samples were vortexed for 10 sec. followed by centrifugation at 2,800 g for 5 min. at 4° C. The supernatants were carefully removed (cytosolic fraction) and pellet were resuspended with 500 µL (1 x 10^6 cells/50 µL) of working extraction buffer on ice for 10 min. and vortexed occasionally. The resuspended samples were sonicated 2 × 20 sec. The samples were cooled on ice between sonication pulses for 30 sec., and centrifuged at 16,000 g at 4°C for 10 min. The supernatants were transferred to a new tube, and chromatin buffer was added at a ratio of 1:1. The extracts were then used for SDS-PAGE and the proteins were detected by Western blotting.

Immunoprecipitation

Immunoprecipitation experiments were performed as described before (41,42). Briefly, 15 x 10^6 cells were collected upon completion of incubation. Cells were washed twice with 1X PBS and centrifuge at 3000 g for 5 min. Pellets were subjected to lysis using IP lysis buffer. Lysate were precleared using Dynabeads™ Protein A (cat# 10001D, Invitrogen) and followed by incubation

with Anti-HA Magnetic beads (cat# 88837, Pierce) for 16-18 hrs. at 4°C. Next, beads were washed twice with lysis buffer, once with PBS. Purified proteins were eluted SDS sample buffer by incubating for 5 minutes at 95°C. Proteins were resolved on SDS-PAGE and detected by Western blotting.

Western Blotting

Total cell, nuclear or chromatin protein fractions were mixed with 5x sample loading buffer (Thermo Fisher cat# 39000) to dilute the buffer to 1x. The mixture was then heated at 95-100°C for 5 min. to denature protein and loaded onto 4-12% GenScript SurePAGE™ Precast Gels (GenScript cat# M00653). The electrophoresis was run in Tris-MOPS-SDS running buffer (GenScript cat# M00138) at 200V for 30-40 min. After SDS-PAGE electrophoresis, proteins were transferred into nitrocellulose membrane followed by washing twice for 5 min. with MilliQ water to completely remove transferring buffer and blocking in 5% BSA in PBST for one hour. The membranes were incubated overnight at 4°C with primary antibody diluted 1:1000 in 5% BSA/PBST. The membrane was then washed three times by PBST and incubated with the secondary antibody diluted (1:5000) in 5% BSA/PBST for one hour. The procedure was continued by washing membrane three times with 1x PBST and using Pierce ECL Western Blotting Substrate (Thermo Fisher cat# 32106). The protein bands were visualized by iBright.

Immunofluorescence (IF) and confocal microscopy

Cells were processed and analyzed for IF as described before (18). Briefly, cells were fixed with 4% (v/v) paraformaldehyde for 20 min. at 4°C. Then, cells were washed with PBS, permeabilized with 0.5% (v/v) Triton X-100 for 10 min and blocked with PBS containing 3% BSA. Cells were incubated overnight at 4°C with 3% BSA in PBS containing respective primary antibodies followed by washing 3x with PBST buffer and 1 hour incubation with secondary antibodies. After incubation, cells were washed 5x in PBST for 3 min., followed by mounting on a coverslip with 20 µl mounting solution. Cells were visualized and imaged using a Leica SP8

Confocal microscope at a 63X objective magnification, and images were analyzed using ImageJ software. For quantification, > 50 cells were counted from two independent experiments/group. Z-stacking (5 slices per Z-stack with 1 μm) was performed to assess the protein-protein co-localization.

Protein stability assay

Protein stability was analyzed as described before (18). Briefly, cells were treated with 20 μg/mL cycloheximide (CHX) (Selleckchem, cat# S7418) for the indicated time points. Total cell lysates were analyzed by SDS-PAGE electrophoresis followed by Western blotting.

Neutral comet assay

DSBs were detected by neutral comet assay as described before (36). Briefly, comet assays were performed using the Oxiselect Comet Assay Kit (Cell Biolabs, cat# STA-355) according to the manufacturer's instructions. Images were acquired by an inverted Olympus IX70 fluorescence microscope using an FITC filter, and the percentage of tail DNA of individual cells was calculated using the OpenComet plugin of ImageJ.

TMEJ assays

DPC-TMEJ activity was detected as described before (18). Chromosomal TMEJ activity was measured as described before with modifications (43). Briefly, 3 x 10^4 cells were transfected with 5μg Flag-Cas9, 5μg sgRosa26 and 1μg pEGFP-N2 with a Neon transfection kit (Invitrogen, cat# MPK 10025) using 1400 V, 10 ms pulse. Twenty-four hours after transfection, a portion of cells were analyzed for transfection efficiency, and genomic DNA was extracted from remaining cells. Droplet genomic PCR was performed to detect TMEJ products.

BrdU/PCNA assay

DNA end resection was examined as described before (44).

DNA fiber assay measuring replication fork restart/progression.

DNA fiber assay performed as described previously with modifications (45). Briefly, cells were treated or not with 12.5 μM ART558 for 24 hrs. to inhibit TMEJ (18) followed by stepwise incubation with 50 μM CldU (40 min.), 4 mM HU (4 hrs.) and 250 μM IdU (40 min.) in the presence of ART558. Cells were washed 3 x with PBS between each incubation step. Then, cells were harvested, resuspended in 1X PBS at concentration of 1000 cells/μl. 2 μl of cell solution was lysed on slides (Superfrost Plus microscope slides, Fisher Scientific, cat# 12-550-15) with 200 mM Tris–HCl, 50 mM EDTA, 0.5% SDS, pH 7.4 buffer for 8 min. Slides were tilted to a 15-degree angle to spread fibers followed by air drying and fixing in 3:1 methanol: acetic acid for 10 min and 1 wash with H_2O followed by air dry. Then, slides were stored at -20° C until further use. Next, denaturation of DNA fibers was performed in 2.5 M HCl for 2.5 hrs. followed by two times washing with PBS for 5 min. before and after denaturation. Slides were then incubated with BSA solution (2% in PBS) for 40 min. at room temperature prior to incubation with primary antibodies recognizing CldU (Abcam, cat# ab6326, dilution 1:300) and IdU (BD Biosciences, cat# 347580, dilution 1:100) for 2.5 h at room temperature, 3 times washed, then incubated with AlexaFluor488 and AlexaFluor594 conjugated secondary antibodies (ThermoFisher Scientific, cat# A11062 and A21470, respectively, dilutions 1:300) for 1 hour at room temperature. Fibers were mounted after 3 washes with PBS. Images were acquired with a Leica SP8 LSM Confocal microscope and fiber lengths were measured using ImageJ software. A minimum of 100 replication forks were measured per group and DNA fiber lengths are presented as IdU/CldU length ratio.

DNA fiber assay measuring ssDNA gaps.

S1 nuclease assay was performed as described previously (46). Briefly, cells were treated or not with 12.5 μM ART558 for 24 hrs. to inhibit TMEJ (18) and incubated with 50 μM CIdU for 40 min to label replication forks, followed by 250 μM IdU 2 hrs. in the presence or absence of ART558. Subsequently, cells were permeabilized with CSK buffer (100 mM NaCl, 10 mM

MOPS, 3 mM MgCl2, pH 7.2, 300 mM sucrose, and 0.5% Triton X-100) at room temperature for 8 minutes, followed by S1 nuclease treatment (20U/µL) in S1 buffer (30 mM sodium acetate, pH 4.6, 10 mM zinc acetate, 5% glycerol, and 50 mM NaCl) for 30 min. at 37^0C. Finally, cells were collected, pelleted, and resuspended in 100–500 µL PBS at concentration 1-2 x 10^3; 2 µl of cell suspension was spotted on a positively charged slide and lysed and processed as described in the DNA fiber assay section above.

Single-Molecule Analysis of Resection Tracks (SMART)

SMART assay were performed as described previously (47). Briefly, cells were treated with 100 µM CldU for 24 hrs followed by Irradiated at 3 Gy and incubated for 3 hrs. Cells were collected and washed with ice-cold PBS. Resuspend cells at concentration of 1 x 10^3 cells/µL. 2 x 10^3 cells were lysed on slides directly (Superfrost Plus microscope slides, Fisher Scientific, cat# 12-550-15) with 7.5 µL of lysis buffer (200 mM Tris–HCl, 50 mM EDTA, 0.5% SDS, pH 7.4). Slides were tilted 15-degree to spread fibers followed by air dried and fixed in 3:1 methanol: acetic acid for 10 min. Slides were dipped in H_2O and air dried followed by store at -20^0 C overnight. Next day slides were washed with PBS for 5 min. and blocked with 2% bovine serum albumin (BSA) in PBS for 40 min at room temperature prior to incubation with primary antibodies recognizing CldU (Abcam, catalog# ab6326, dilution 1:300) for 2.5 hrs at room temperature. Slides washed with PBS three times, then incubated with AlexaFluor488 conjugated secondary antibodies (ThermoFisher Scientific, cat# A11062, dilutions 1:300) for 1 hr. at room temperature. Images were acquired with a Leica SP8 LSM Confocal microscope and fiber lengths measured using ImageJ software.

DNA dot blot

This method was employed to detect the reduction in the formation of 5-methylcytosine (5-mC) after using DNMT3A inhibitor in the cells, and it was conducted as described before (22). Briefly, cells were treated with DNMT3A-IN-1 (MedChemExpress cat# HY-144433) for 6 days, followed

by genomic DNA (gDNA) extraction. Then, gDNA samples were further diluted to 60 ng/µL. gDNA (2.0, 1.5, 1.0, and 0.5 µg) was prepared in total volume of 100 µL of nuclease-free water. Then, 100 µL of 2x DNA denature buffer was added into gDNA, before the denaturation step at 96-100^{0}C for 10 minutes. The denaturation was terminated by adding 200 µL of ice-cold 2M ammonium acetate (pH 7), and chilled on ice for 5 minutes. The entire DNA mixture was loaded through BioRad Dot Blot apparatus until all the wells were completely vacuumed. The membrane was briefly washed in 2x Saline Sodium Citrate Buffer, and DNA-membrane crosslink was performed under UV on 2 minutes. The membrane was then blocked in 5% non-fat dry milk in PBST for 1 hour and incubated overnight with anti- 5-mC primary antibody (Cell Signaling, cat# 28692) diluted (1:1000) in 5% BSA in PBST at 4^0 C. The following day, the membrane was washed in PBST and incubated for 1 hr. with HRP-conjugated antibody diluted 1:5000 in 5% BSA in PBST before adding the Pierce ECL Western Blotting Substrate to visualize the dot blot using iBright.

***Polq* RT-PCR**

Total RNA was extracted from 10^7 cells. The cells were lysed in 600 µL TRI-Reagent (MRC cat# TR-118) to obtain RNA, DNA and proteins. Then, the equal volume of 100% ethanol was added to precipitate RNA and DNA. Genomic DNA was removed, and total RNA was washed and purified by Zymo Research R2050 Direct-zol RNA MiniPrep (Genesee cat# 11-330). The purification and concentration of RNA were measured by NanoDrop Spectrophotometer (Thermo Scientific cat# ND-1000). Genomic DNA removal was validated by agarose (1% w/v) electrophoresis. Next, 3 µg total RNA was employed to synthesize cDNA by SuperScript™ IV First-Strand Synthesis System (Thermo Scientific cat# 18091050). Basically, RNA was annealed to Oligo d(T)$_{20}$ primer, and cDNA was synthesized by reverse transcriptase enzyme. In the last step, the remaining RNA was removed by *E. coli* RNase H. In the PCR reaction, 1.5 µL of cDNA template was added to 2X DreamTaq Green PCR Master Mix (Thermo Scientific

cat# K1082), 1 µM forward primer, 1 µM reverse primer, and nuclease-free water to obtain the total reaction volume up to 25 µL. Nuclease-free water was used to replace cDNA template as the negative control. Thermocycler included initial denaturation at 95^0C in 3 min.; followed by 36 cycles of 95^0C in 1 min., 58^0C in 45 sec., and 72^0C in 2 min.; and the final extension at 72^0C in 10 min. Finally, PCR products were evaluated by agarose (1% w/v) electrophoresis.

List of primers used in *Polq* RT-PCR.

Name of primer		**Sequence (5' – 3')**
Polq1	Forward	CGGGAGGCCTATGGGACTGT
	Reverse	GTGCACAGGCTCCAGAGATCC
Polq2	Forward	CATCGAAGGAGCCTTCCGTC
	Reverse	CTATGCCTCGCTCTGCATCTG
Polq3	Forward	CTGGCAAGGGCTTATCTGCAAG
	Reverse	GACTGGAGCGCCTCTATTGATG
Polq4	Forward	GCTGGTAGTAGTTATGTGGCCA
	Reverse	AGCACTGCTGGCTTTCTGACG
Polq5	Forward	TGGGGACAGTTCAGAGAACTTC
	Reverse	CCTGGTAAAGGATGCAAGCCCT
Polq6	Forward	AGTACTGCCTGGCCTTGCTAGA
	Reverse	GCTCTGGGGATCTGGTTAACTGT
Polq7	Forward	TGAGGATCCTGGCTCACTTGTC
	Reverse	CAGGCACTAAGGGGCTAGCTAG

CpG bisulfite amplicon sequencing of murine *Polq*

Genomic DNA (250 to 500 ng) of the FD and FT cells was converted by sodium bisulfite using the EZ DNA Methylation-Lightning kit (Zymo Research) according to the manufacturer's instructions. PCR was used to amplify the converted DNA using the following primer pairs: 5′-TTTAGTTAGGAGAATTTTGTGGTTT-3′ plus 5′-AATAACAACCCTACCTCCAACTATC-3′. PCR products were sent to the Massachusetts General Hospital Center for Computational and Integrative Biology DNA Core Facility for amplicon sequencing. After trimming adapter sequencing, the sequences of interest were aligned to the converted mm39 genome using Bowtie2 and Bismark; bedgraph files were then extracted to graph, in Integrative Genomics Viewer, the percent methylation corresponding to each of the CpG locations.

Promoter transactivation assay

The cells were cultured in Iscove-modified Dulbecco medium growth medium supplemented with 10% FBS, 1% L-glutamine, 1x Penicillin/Streptomycin and 1% WEHI-conditioned medium. After 24 hrs. the cells were transfected by nucleofection (Lonza Amaxa kit V, cat# VCA-1003). To this end, 1 x 10^6 of cells and 1.5 μg of plasmid obtained from GeneCopoeia with *POLQ* promoter [NM_001159369 (cat# MPRM33982-PG04)] were used for nucleofection following the manufacturer protocol. After nucleofection, the cells were transferred to 3 mL of growth medium without antibiotics. Activity of Gaussia luciferase and Alkaline Phosphatase secreted to medium was measured after 48 hrs. using Secrete-Pair Dual Luminescence Assay Kit (GeneCopoeia, cat# LF032), following the manufacturer protocol.

3'UTR regulation luciferase assay

The assay was performed as described before (18). Briefly, cells were seeded in Iscove-modified Dulbecco medium supplemented with 10% FBS, 1% L-glutamine, Penicillin/Streptomycin, and 10% WEHI-conditioned medium. After 24h the cells were transfected by nucleofection (Amaxa SF Cell line 4D-Nucleofector X kit L, cat# V4XC-2024). To this end 1 x 10^6 cells and 2 μg of plasmid obtained from GeneCopoeia: control (#CmiT000001-MT06), *Polq* 3'UTR of NM_029977.2 (#MmiT106208-MT06) or *Parp1* 3'UTR of NM_007415.3 (#MmiT090879-MT06), were used for nucleofection following the manufacturer protocol. After nucleofection the cells were transferred to 3 mL of growth medium supplemented with 10% WEHI and 10% FBS but without antibiotics. The activity of firefly and Renilla luciferases was checked after 18 hrs. using the Duo-Luciferase Assay kit (Promega, cat# E1910), following the manufacturer's protocol.

mRNA stability assay

Cells (3.5 x 10^6) were simultaneously treated with 5 μg/mL actinomycin D (Selleckchem cat# S8964) and 2 μg/mL cycloheximide (Selleckchem cat# S7418) for 0, 1 and 2 hours followed by

washing twice with ice-cold PBS. Cells were lysed in 350 µL TRI-Reagent (MRC, cat# TR-118), total RNA was purified, and cDNA was synthesized by RT-PCR. The quantitative RT-PCR of *Polq* was performed, following the procedure described in *Polq* RT-qPCR. The expression of *Parp1* (ThermoFisher Scientific, cat# Mm01321084_m1) was used as a control.

Real-time RT-qPCR

RNA was extracted using RNeasy plus mini kit (Qiagen, cat# 74134), following the manufacturers guidelines. The isolated RNA was redissolved in Milli-Q water. Extracted RNA was converted to cDNA using SuperScript IV first-strand synthesis system (Invitrogen #18091050) using manufacturer's protocol. Predesigned TaqMan assay (Polq Assay ID: Mm00712819_m1) and TaqMan gene expression master mix (Applied Biosystems Assay ID# 4369016) were used for quantitative real-time RT-PCR. Briefly, 5 µl of TaqMan gene expression master mix, 0.5µL TaqMan assay, and 1.5µL cDNA and 3µL nuclease-free water were used for qPCR. The housekeeping gene, ubiquitin C (*Ubc*) (Thermo Fisher Scientific, Assay ID# Mm01201237_m1) was used to normalize gene expression. The thermocycle was established by a default program for *Taqman* chemical reaction in the QuantStudio Real-Time PCR 96-well Instrument (ThermoFisher Scientific). The relative gene expression level was calculated by using comparative ΔCt ($Ct_{Polq} – Ct_{UBC}$) analysis.

Cell cycle analysis

Cells were maintained in the indicated culture medium for 24 hours. Then, the cells were collected and washed twice by 1X PBS buffer + 2% FBS, followed by the incubation with 80% ethanol in 2 hours at -20°C for permeability. In the last step, after washing ethanol by 1X PBS buffer + 2% FBS, the permeable cells were incubated with PE-conjugated PI/RNase staining buffer (BD BioSciences #550825) for 15 minutes at RT before analyzing in flow cytometry. As the outcome, proportion of G_o-G_1, S and G_2-M phases was calculated by FlowJo software.

***In vivo* treatment**

Ten-week old female NRG mice (The Jackson Laboratory, cat# 007799) were total body irradiated (4 Gy) and injected i.v. with 1 x 10^3 GFP^+ FLT3(ITD);*Dnmt3a*^{KD} 32Dcl3 cells. The treatment regimen began when the percentage of GFP^+ cells in peripheral blood leukocytes (PBL) reached 5-10%. Mice (10 mice/group) were randomized and treated for 14 consecutive days with (1) vehicle, (2) RP-6685 [80 mg/kg oral gavage (48)], (3) etoposide [5 mg/kg every two days (49)], and (4) the combination of etoposide and RP-6685. The efficacy of the treatment was evaluated by measurements of GFP^+ cells in PBL and the median survival time was determined.

Statistics

Data are expressed as mean ± standard deviation (SD) from at least 3 independent experiments unless stated otherwise. When conducting subgroup comparisons between two groups, two-tailed unpaired t-test was used for normally distributed variables. Multiple groups were compared using one-way Anova. Median survival time of the mice ± standard error (SE) was calculated by Kaplan-Meier and compared by Log-Rank test. p values less than 0.05 were considered statistically significant; *$p<0.05$, **$p<0.01$, ***$p<0.001$ and ****$p<0.0001$.

Institutional approvals

The patient samples were collected after obtaining informed consent in concordance with the Declaration of Helsinki and were approved by the institutional review boards. Animal experiments were approved by the Institutional Animal Care and Use Committees review board at Temple University. Mice were housed in a temperature- and light-controlled animal facility under a 12-h light/dark cycle and were provided standard food and water ad libitum.

Results

DNMT3A deficient malignant hematopoietic cells are addicted to Polθ.

FLT3(ITD)-positive murine hematopoietic 32Dcl3 cells and isogenic cells lacking TET2 [FLT3(ITD);*Tet2*^{KD}] or DNMT3A [FLT3(ITD);*Dnmt3a*^{KD}] were screened for their sensitivity to

doxorubicin and DDR inhibitors targeting various aspects of DSB repair (Figure 1A). As expected, FLT3(ITD);*Dnmt3a*^{KD} cells were resistant to doxorubicin and PARPi when compared to FLT3(ITD) and FLT3(ITD);*Tet2*^{KD} counterparts (Figure 1B) (6,22). Moreover, FLT3(ITD);*Dnmt3a*^{KD} cells displayed resistance to most of the tested DDR inhibitors in concordance with our recent report involving AML patient cells (50). The high overall toxicity of the RAD51 inhibitor most likely resulted from inhibition of HR, a key DSB repair pathway in proliferating cells (19).

Remarkably, FLT3(ITD);*Dnmt3a*^{KD} 32Dcl3 cells were selectively highly sensitive to five different Polθ inhibitors which reduced TMEJ: ATPase inhibitor novobiocin (NVB), and DNA polymerase inhibitors ART558, ART812, RP-6685 and RTx-161, when compared to FLT3(ITD) and FLT3(ITD);*Tet2*^{KD} counterparts (Figure 1C, D) (18,38,48,51-53). In addition, murine Lin-cKit+ *Flt3*$^{ITD/ITD}$;*Dnmt3a*$^{-/-}$ bone marrow cells were more sensitive to Polθi ART812 when compared to their *Flt3*$^{ITD/ITD}$ counterparts (Figure 1E). Importantly, human Lin-CD34+ *FLT3*^{ITD};*DNMT3A*^{R882H} AML primary cells were highly sensitive to ART812 when compared to *FLT3*^{ITD} patient cells (Figure 1F). In addition, *JAK2*^{V617F};*DNMT3A*^{R882H} SET-2 cells and murine Lin^{-}cKit^{+} *Flt3*$^{ITD+/-}$;*Dnmt3a*$^{R882H/+}$ cells displayed sensitivity to ART558 when compared to JAK2^{V617F} and *Flt3*$^{ITD+/-}$ cells, respectively (Figure 1G, H). Also, inhibition of DNMT3A activity in FLT3(ITD) 32Dcl3 cells by a selective small molecule inhibitor DNMT3A-IN-1 [validated by reduction of 5-mC (Figure 1I, right panel)] resulted in increased sensitivity to Polθi (Figure 1I, left panel). Of note, FLT3(ITD);*Tet2*^{KD} 32Dcl3 cells, *Flt3*$^{ITD/ITD}$;*Tet2*$^{-/-}$ mBMCs, and human FLT3(ITD);*TET2mut* AML primary cells were resistant to NVB, ART558, ART812 and RP-6685 (Figure 1D-F).

ART558 treatment of FLT3(ITD);*Dnmt3a*^{KD} 32Dcl3 cells resulted in accumulation of DSBs detected by neutral comet assay (Figure 1J) supporting the hypothesis that inhibition of TMEJ led to accumulation of toxic DSBs. Polθi ART558 exerted its anti-leukemia activity, at

least partially, by activating DNA damage-dependent pro-apoptotic cGAS-STING pathway because STING inhibitor (STINGi) C-176 reduced the growth inhibitory effect of Polθi ART558 in FLT3(ITD);*Dnmt3a*^{KD} 32Dcl3 cells (Figure 1K, left panel) (54). As expected, treatment with ART558 induced phosphorylation of TBK1 [a marker of active STING (55)] in FLT3(ITD);*Dnmt3a*^{KD} 32Dcl3 cells, which was inhibited by C-176 (Figure 1K, right panel).

Next, we determined the source of spontaneous DSBs in FLT3(ITD);*Dnmt3a*^{KD} 32Dcl3 cells. We reported that in leukemia cells enhanced production of formaldehyde by serine/1C cycle metabolism and reactive oxygen species (ROS) by mitochondrial respiratory chain resulted in increased numbers of formaldehyde-induced DNA protein crosslinks (DPCs) and oxidative DNA lesions such as 8-oxoguanine (8-oxoG), respectively; unresolved DPCs and 8-oxoG may produce DSBs (18,56). We show here that FLT3(ITD);*Dnmt3a*^{KD} 32Dcl3 cells and Lin^{-}cKit^{+} *Flt3*$^{ITD/ITD}$;*Dnmt3a*$^{-/-}$ mBMCs accumulate more formaldehyde and/or DPCs when compared to FLT3(ITD) and also FLT3(ITD);*Tet2*^{KD} counterparts (Supplemental Figure S2A,B). Since *Dnmt3a*^{KD} did not enhance the expression of SPRTN protease and TDP1 and TDP2 hydrolases (Supplemental Figure S2C), the proteins directly involved in DPCs removal (57), it is unlikely that they provide sufficient protection against abundant DPCs in DNMT3A-deficient leukemia cells. Unresolved DPCs will ultimately generate DSBs likely contributing to the hypersensitivity to Polθ inhibitors (18,58). In keeping with this, FLT3(ITD);*Dnmt3a*^{KD} 32Dcl3 cells were resistant to Polθ inhibitor when cultured in glucose-, serine-, and glycine-free medium (No GSG) which abrogated serine/1C cycle metabolism-mediated generation of formaldehyde-induced DPCs (Supplemental Figure S2D, left) (18). Conversely, FLT3(ITD);*Dnmt3a*^{KD} 32Dcl3 cells remained hypersensitive to Polθ inhibitor in high glucose-, serine-, and glycine- culture medium (High GSG) which facilitated production of formaldehyde and accumulation of DPCs (Supplemental Figure S2D, right). FLT3(ITD);*Dnmt3a*^{KD} 32Dcl3 cells, however, did not accumulate more ROS and 8-oxoG lesions when compared to FLT3(ITD) and FLT3(ITD);*Tet*^{KD}

counterparts (Supplemental Figure S2E and F, respectively). Thus, it is likely that Polθ plays a major role in the repair of DPCs - but not ROS -induced DSBs to promote survival of FLT3(ITD);*Dnmt3a*^{KD} 32Dcl3 cells.

To obtain additional evidence about the role of Polθ in *DNMT3A*-mutated hematological malignancies, Polθ was inactivated by introducing a point mutation in *Polq* exon 1 to create a premature stop codon (*Polq*$^{-/-}$ mice) and by expression of Polθ D2230A+Y2231A polymerase inactive mutant. While deletion of *Polq* gene did not affect clonogenic potential of *Dnmt3a*$^{-/-}$ mBMCs, it had a detrimental effect on the clonogenic activity of the cells transformed with FLT3(ITD), JAK2(V617F) and BCR-ABL1 oncogenic tyrosine kinases (Figure 2A). This effect was associated with elevated DSBs (γH2AX) and decreased engraftment of GFP^{+};FLT3(ITD);*Dnmt3a*$^{-/-}$;*Polq*$^{-/-}$ cells in mice when compared to GFP^{+};FLT3(ITD);*Dnmt3a*$^{-/-}$ counterparts (Figure 2B and C, respectively).

Polθ could be also inactivated by the expression of D2230A+Y2231A polymerase-deficient mutant which exerts a dominant-negative effect (59). We found that clonogenic activity of Lin^{-}cKit^{+} GFP^{+};*Flt3*$^{ITD+/-}$;*Dnmt3a*$^{R882H/+}$ mBMCs transduced with Polθ(D2230A+Y2231A) mutant was decreased when compared to these transduced with wild-type Polθ (Figure 2D). This effect was accompanied by accumulation of DSBs (γH2AX) in the former cells (Figure 2E). In addition, reduction of clonogenic activity by Polθ(D2230A+Y2231A) mutant was also detected in RFP^{+};FLT3(ITD);*Dnmt3a*^{KD} 32Dcl3 cells (Figure 2F). When injected into SCID mice, Polθ(D2230A+Y2231A) mutant abrogated the engraftment and leukemogenic capability of RFP^{+};FLT3(ITD);*Dnmt3a*^{KD} 32Dcl3 cells (Figure 2G, H).

Altogether, we present comprehensive evidence in orthogonal but complementary systems that inactivation of Polθ is selectively detrimental to DNMT3A-deficient myeloid hematological malignancies. This effect is associated with accumulation of formaldehyde-induced DPCs-triggered toxic DSBs and activation of cGAS/STING pathway.

Inactivation of DNMT3A enhances Polθ expression by downregulation of PARP1-mediated PARylation-dependent ubiquitination (PARdU) of Polθ by UBE2O E3 ligase.

Western blot analyses revealed abundant overexpression of Polθ protein in FLT3(ITD);*Dnmt3a*^{KD} 32Dcl3 cells, and in Lin^{-} FLT3(ITD);*Dnmt3a*$^{-/-}$ and *Flt3*$^{ITD+/-}$;*Dnmt3a*$^{R882H/+}$ mBMCs when compared to *Dnmt3a* wild-type counterparts (Figure 3A). Of note, Polθ was almost undetectable in FLT3(ITD);*Tet2*^{KD} 32Dcl3 cells and *Flt3*$^{ITD/ITD}$;*Tet2*$^{-/-}$ mBMCs, explaining their resistance to Polθi (Figure 1C, D). In addition, incubation of FLT3(ITD) 32Dcl3 cells with DNMT3A inhibitor elevated Polθ expression (Figure 3B). Polθ was also elevated in DNMT3A-deficient cells expressing JAK2(V617F) and MPL(W515L) oncogenic tyrosine kinases (Supplemental Figure S3A) and in HCC-15 and A549 lung carcinoma cells treater for 6 days with DNMT3Ai (Supplemental Figure S3B), implicating a more general role of DNMT3A in regulating Polθ expression in hematological malignancies and solid tumors.

We did not detect any significant differences in *Polq* promoter region methylation between FLT3(ITD), FLT3(ITD);*Dnmt3a*^{KD}, and FLT3(ITD);*Tet2*^{KD} 32Dcl3 cells (Supplemental Figure S3C). In addition, DNMT3A-deficient leukemia cells displayed a modest 20-35% enhancement of *Polq* mRNA expression (Supplemental Figure S3D) which was associated with increased *Polq* mRNA stability (Supplemental Figure S3E), but not with stimulation of promoter transactivation and/or alternative splicing (Supplemental Figure S3F and G, respectively). In addition, 30-40% enhancement of Polθ protein translation (Supplemental Figure S3H) was also detected in DNMT3A-deficient leukemia cells. These rather modest increases of the mRNA stability and protein translation were unlikely to explain 4-5 -fold and a remarkable 10-34 -fold overexpression of Polθ protein in DNMT3A deficient leukemia cells when compared to DNMT3A proficient and to TET2 deficient counterparts, respectively (Figure 3A, Supplemental Figure S3I).

Intriguingly, PARP1 expression was inversely proportional to Polθ levels in FLT3(ITD), JAK2(V617F) or MPL(W515L) -positive DNMT3A-deficient cells when compared to DNMT3A proficient and to TET2 deficient counterparts (Figure 3A, B, Supplemental Figure S3A), suggesting that PARP1 might repress Polθ expression. To test this hypothesis, PARP1 was downregulated by shRNA in FLT3(ITD)-positive 32Dcl3 cells, which caused upregulation of Polθ (Figure 3C). Moreover, *FLT3*^{ITD}*;Parp1*$^{-/-}$ mBMCs displayed higher expression of Polθ when compared to *FLT3*^{ITD}*;Parp1*$^{+/+}$ counterparts (Figure 3D). Conversely, ectopic overexpression of PARP1 in FLT3(ITD);*Dnmt3a*^{KD} 32Dcl3 (FLT3(ITD);*Dnmt3a*^{KD} + PARP1) cells resulted in downregulation of Polθ (Figure 3E).

Downregulation of PARP1 in FLT3(ITD);*Dnmt3a*^{KD} 32Dcl3 cells likely depended on decreased PARP1 translation (Supplemental Figure S4A) and reduced protein stability (Supplemental Figure S4B) associated with proteasomal degradation (Supplemental Figure S4C). Among E3 ligases reported to be involved in PARP1 degradation (60-63), HUWE1 was selectively upregulated in FLT3(ITD);*Dnmt3a*^{KD} 32Dcl3 cells when compared to FLT3(ITD);*Tet2*^{KD} and FLT3(ITD) counterparts (Supplemental Figure 4D) and co-immunoprecipitated with PARP1 (Supplemental Figure 4E). Remarkably, shRNA-mediated downregulation of HUWE1 rescued PARP1 and abrogated Polθ proteins expression in FLT3(ITD);*Dnmt3a*^{KD} 32Dcl3 cells (Supplemental Figure 4F). At the same time *PARP1* methylation, mRNA expression and stability were not affected by DNMT3A deficiency (Supplemental Figure S4G-I).

Downregulation of PARP1 in FLT3(ITD) 32Dcl3 cells did not increase *Polq* mRNA stability and Polθ translation (Supplemental Figure S4J and K, respectively). In concordance, *in silico* analysis did not detect PARP1 binding sites in any region of *POLQ* exon, intron, promoter, or 3'UTR sites, using the published ChIP and ATAC-Seq datasets deposited in the GeneHancer

database (https://academic.oup.com/database/article/doi/10.1093/database/bax028/3737828). Thus, Polθ appeared to be regulated by another PARP1-dependent mechanism.

PARP1-mediated downregulation of Polθ is a rapid and efficient process which depends on PARP1 catalytic activity, because PARP1 specific inhibitor enhanced the levels of Polθ in FLT3(ITD) and FLT3(ITD);*Dnmt3a*^{KD} + PARP1 32Dcl3 cells in less than 5 min (Figure 3F), suggesting that PARylated Polθ is targeted for degradation. In support of this hypothesis, PARylation of Polθ immunoprecipitated from FLT3(ITD);*Dnmt3a*^{KD} 32Dcl3 cells was strongly reduced when compared to that immunoprecipitated from FLT3(ITD) counterparts (Figure 3G).

The speed and robustness of PARP1-mediated repression of Polθ expression implicated proteasomal degradation (64). In concordance, while Polθ was downregulated in FLT3(ITD);*Dnmt3a*^{KD} + PARP1 32Dcl3 cells, proteasome inhibitor increased the expression of TP53 [positive control, (65)] and rescued the overexpression of Polθ (Figure 3H). Moreover, Polθ was found in anti-Ub immunoprecipitates from FLT3(ITD) cells, but not from FLT3(ITD);*Dnmt3a*^{KD} 32Dcl3 counterparts (Figure 3I). Altogether, abrogation of PARP1-mediated PARylation of Polθ in FLT3(ITD);*Dnmt3a*^{KD} 32Dcl3 cells resulted in its decreased ubiquitination and reduced proteasomal degradation.

To identify the E3 ligase responsible for ubiquitination of Polθ, we analyzed a pull-down of Polθ followed by LC-MS/MS and detected UBE2O E3 ligase as a potential partner of Polθ (66). UBE2O was modestly downregulated in FLT3(ITD);*Dnmt3a*^{KD} cells when compared to FLT3(ITD) and FLT3(ITD);*Dnmt3a*^{KD} + PARP1 32Dcl3 cells (Figure 3J, Input). Remarkably, UBE2O was not detected in anti-Polθ immunoprecipitates from FLT3(ITD);*Dnmt3a*^{KD} cells, while it was readily detectable in those from FLT3(ITD) and FLT3(ITD);*Dnmt3a*^{KD} + PARP1 32Dcl3 counterparts (Figure 3J, IP-Polθ). To determine if UBE2O is responsible for PARP1-mediated degradation of Polθ in leukemia cells, expression of UBE2O was knocked down by siRNA in FLT3(ITD);*Dnmt3a*^{KD} + PARP1 32Dcl3 cells (Figure 3K). This effect was associated with

upregulation of Polθ without affecting PARP1 expression. Moreover, inhibition of PARP1 activity resulted in dissociation of Polθ-UBE2O complex and elevated expression of Polθ (Figure 3L). Altogether, we postulate that DNMT3A deficiency in FLT3(ITD)-positive leukemia cells promoted overexpression of Polθ by abrogation of PARdU-dependent UBE2O E3 ligase-mediated ubiquitination and proteasomal degradation of Polθ.

Since we reported that FLT3(ITD) kinase stimulates ERK1/2 kinase to protect Polθ from c-CBL E3 ligase-mediated ubiquitination and proteasomal degradation (18), we examined if FLT3(ITD)-ERK1/2 axis plays a role in regulating Polθ expression in FLT3(ITD);*Dnmt3a*^{KD} 32Dcl3 cells. Inhibition of FLT3(ITD) kinase or ERK1/2 kinase only modestly reduced Polθ expression in FLT3(ITD);*Dnmt3a*^{KD} 32Dcl3 cells whereas it exerted a strong inhibitory effect in FLT3(ITD) counterparts (Supplemental Figure S5A and B, respectively). Therefore, we tested if downregulation of PARP1 and activations of ERK1/2 kinase work in concert to upregulate Polθ in DNMT3A deficient leukemia cells. For this reason, PARP1 was ectopically expressed and/or ERK1/2 kinase was inhibited in FLT3(ITD);*Dnmt3a*^{KD} 32Dcl3 cells. Western blot analysis revealed that Polθ expression was almost completely abrogated by the combined effect of ectopic expression of PARP1 and inhibition of ERK1/2 kinase (Supplemental Figure S5C). In conclusion, we postulate that DNMT3A deficiency-dependent inhibition of PARP1-PARdU-UBE2O and FLT3(ITD) kinase-mediated regulation of ERK1/2-c-CBL pathways contributed to abundant expression of Polθ in DNMT3A-deficient leukemia cells (Supplemental Figure S5D).

Polθ-dependent DNA repair is enhanced in DNMT3A deficient leukemia cells.

Next, we examined if abundant overexpression of Polθ in *DNMT3A*mut leukemia cells results in enhanced DNA repair. Intracellular recruitment of Polθ to DNA damage could be detected in the form of nuclear foci (67-69). Polθ foci formation was tested in untreated cells [spontaneous DSBs caused by metabolic products: ROS and formaldehyde, and by replication stress (15-18)]

and in cells receiving 2 Gy of γ-irradiation. Immunostaining followed by confocal microscopy revealed that FLT3(ITD);*Dnmt3a*^{KD} cells accumulated 5x and 2x more spontaneous and irradiation-induced Polθ foci, respectively, when compared to FLT3(ITD) counterparts (Figure 4A), implicating enhancement of Polθ-mediated DNA repair in the former cells. As expected, Polθ foci were almost undetectable in FLT3(ITD);*Tet2*^{KD} cells which express very low levels of Polθ (Figure 3A).

We recently described a two-step spatiotemporal mechanism of Polθ regulation by PARP1 and PARG (66). First, PARP1 PARylates Polθ and facilitates its recruitment to DNA damage sites in an inactivated state. Second, PARG removes repressive PAR marks on Polθ to activate TMEJ. We postulate that the abundance of Polθ expression might alleviate the role of downregulated PARP1 in recruitment of Polθ to DNA damage sites in DNMT3A-deficient leukemia cells. However, it should be noted that reduced PARP1 loading on chromatin (Supplemental Figure S6A) and limited PARylation of Polθ (Figure 3G) in DNMT3A-deficient leukemia cells might provide enough signaling to recruit abundantly expressed Polθ to DNA damage where it is dePARylated and activated by PARG.

Polθ has been reported to play a key role in TMEJ and in restarting of stalled replication forks regardless of HR status, and also in ssDNA gap repair/filling during replication fork progression in HR-deficient cells (25-29). We examined these functions using specific experimental protocols to measure key Polθ-mediated DNA repair activities in *DNMT3A*mut leukemia cells.

To assess TMEJ, we took advantage of the intrachromosomal model whereby cells are transfected with Flag-Cas9 and sgRosa26 to generate a DSB in *Rosa26* murine locus on chromosome 6 (43). TMEJ uses 6-bp or 4-bp microhomology to generate 23-bp or 39-bp deletions, respectively, detected by quantitative droplet digital PCR assay (Figure 4B central panel, TMEJ-del 23bp and TMEJ-del 39bp). Both, TMEJ-del 23bp and TMEJ-del 39bp

amplicons of the DSB in *Rosa26* locus were enhanced in FLT3(ITD);*Dnmt3a*^{KD} 32Dcl3 cells when compared to FLT3(ITD)-positive counterparts (Figure 4B, peripheral panels).

Moreover, we reported that Polθ-mediated TMEJ plays a key role in repairing DSBs resulting from DPCs (58). Thus, DPC-associated DSB repair was measured by a reporter assay carrying a split green fluorescent protein (GFP) construct conjugated with 5′-terminal biotin-streptavidin linkages on both DNA ends (Figure 4C, left panel) (58). TMEJ of the left and right 5′-adducted DNA constructs transduced into the cells is expected to use the 6-bp microhomology tract to restore *GFP* sequence resulting in GFP expression. Using this assay, we detected that FLT3(ITD);*Dnmt3a*^{KD} 32Dcl3 cells and Lin^{-} *Flt3*$^{ITD+/-}$;*Dnmt3a*$^{R882H/+}$ mBMCs displayed >2-fold and >4-fold increased DPC-TMEJ activity when compared to FLT3(ITD)-positive *Dnmt3a* wild-type and FLT3(ITD);*Tet2*^{KD} counterparts, respectively (Figure 4C, middle and right panels, respectively).

The impact of Polθ on replication fork restart and/or progression was examined by DNA fiber analysis (Figure 4D, left panel). Cells were labeled with CldU, followed by hydroxyurea (HU) treatment to stall the forks, and subsequently released into IdU in the presence or absence of Polθi ART558. While fork restart and/or progression activity did not differ between untreated FLT3(ITD), FLT3(ITD);*Tet2*^{KD} and FLT3(ITD);*Dnmt3a*^{KD} cells, ART558 exerted strong (~1.6x) and modest (~1.1x) inhibitory effects in FLT3(ITD);*Dnmt3a*^{KD} and FLT3(ITD) cells, respectively (Figure 4D, middle and right panels). As expected, ART558 did not affect replication fork restart and/or progression in FLT3(ITD);*Tet2*^{KD} cells which express very low levels of Polθ (Figure 3A) and are not sensitive to the inhibitor (Figure 1B).

Polθ-mediated ssDNA gap filling was investigated using modified DNA fiber assay where the gaps were detected by S1 nuclease activity (Figure 4E, left panel). Cells were labeled with the nucleoside analogs CldU and IdU followed by incubation with S1 nuclease to digest regions of ssDNA. S1 nuclease incubation modestly shortened the length of labeled tracks in

FLT3(ITD), FLT3(ITD);*Tet2*^{KD} and FLT3(ITD);*Dnmt3a*^{KD} cells, indicating that ssDNA gaps are not abundant in these cells (Figure 4E, right panel). Importantly, ART558 did not affect the length of labeled tracks suggesting that ssDNA gaps are not processed by Polθ in these cells.

Altogether, we observed that overexpressed Polθ in DNMT3A-deficient cells promoted abundant TMEJ and fork restart, but not ssDNA gap filling.

DNMT3A knockdown limits DSB end-resection to create favorable substrates for TMEJ. The extent of DNA end resection plays a key role in DSB repair choice and is usually determined by the interplay between the Shieldin complex restricting end resection and DNA nucleases promoting end resection (70,71). TMEJ acts on short-range resected ends usually generated by MRE11 and CtIP nucleases, while HR prefers long-range resected ends created by EXO1 nuclease (72) (Figure 5A).

To evaluate end resection, we employed BrdU/PCNA assay where following DNA damage and DNA end resection, the length of single-stranded DNA is specifically estimated by an intensity of anti-BrdU immunostaining in the S/G2 phase of the cell cycle marked by PCNA staining (44) (Figure 5B). Using BrdU/PCNA approach, we observed that the presence of FLT3(ITD) promoted DSB-end resection (Figure 5C), consistent with our previous report (18). Remarkably, *Dnmt3a*^{KD} was associated with reduced end resection in FLT3(ITD)-positive cells. In addition, we applied SMART assay, a modified DNA combing technique, to measure DNA resection at the level of individual DNA fibers (73) (Figure 5D). In concordance with the cellular BrdU/PCNA assay, SMART assay detected that resection of individual DNA fibers was enhanced in FLT3(ITD) cells when compared to parental counterparts, but decreased in FLT3(ITD);*Dnmt3a*^{KD} cells (Figure 5E).

Moreover, we evaluated the accumulation of RPA32 into nuclear foci, a well-established resection marker (74). In concordance with BrdU/PCNA and SMART assays, RPA32 foci formation/intensity was decreased in irradiated FLT3(ITD);*Dnmt3a*^{KD} 32Dcl3 cells when

compared to FLT3(ITD) counterparts (Figure 5F). Finally, we detected decreased accumulation of RAD51 foci, a marker of HR (75), in FLT3(ITD);*Dnmt3a*^{KD} 32Dcl3 cells when compared to FLT3(ITD) counterparts (Figure 5G). Inhibition of RPA32 and RAD51 foci formation in FLT3(ITD);*Dnmt3a*^{KD} 32Dcl3 cells were not due to differences in the protein expressions (Figure 5F and G, insets) and number of DSBs caused by irradiation (Figure 5H). Altogether, we concluded that DNMT3A deficiency restricted DNA end resection in FLT3(ITD)-positive cells.

DNMT3A knockdown disassembles PARP1-SMARCAD1-MSH2/MSH3 repressive complex to facilitate Polθ loading on DSBs

Limited DNA end resection in FLT3(ITD);*Dnmt3a*^{KD} 32Dcl3 cells was associated with decreased association of PARP1 with chromatin (Figure 6A). PARP1 has been reported to affect DNA end resection by regulating the recruitment of MRE11, CtIP and EXO1 nucleases playing a critical role in DSB end processing (Figure 5A) (76,77). However, the presence of all these proteins were similar in chromatin extracts of FLT3(ITD) and FLT3(ITD);*Dnmt3a*^{KD} 32Dcl3 cells (Figure 6A). In addition, chromatin recruitment of REV7 (78), one of key factors of the shieldin complex is not affected by DNMT3A knockdown (Figure 6A). Therefore, it is rather unlikely that these factors contribute to limited DNA end resection in DNMT3A deficient cells.

PARP1 has been also reported to modulate DNA end resection (76,77). Remarkably, PARP1 chromatin localization was downregulated in FLT3(ITD);*Dnmt3a*^{KD} 32Dcl3 cells (Figure 6A). Using SMART assay we detected that an extensive DNA end resection in HR-proficient FLT3(ITD) mBMCs was limited in FLT3(ITD);*Parp1*$^{-/-}$ counterparts (Figure 6B), implicating PARP1 in this process.

PARP1 interacts with the SWI/SNF-like protein SMARCAD1 (79) which recruits MSH2/MSH3 heterodimer to prolong end resection, engaging HR rather than TMEJ (80). Thus, we hypothesized that impaired presence of PARP1 on the chromatin in FLT3(ITD);*Dnmt3a*^{KD} cells might abrogate the recruitment of repressive SMARCAD1-MSH2/MSH3 complex and

facilitate Polθ assembly on DNA damage resulting in limited DNA end resection. To test this hypothesis, SMARCAD1 recruitment to chromatin/DSBs was compared in irradiated FLT3(ITD) and FLT3(ITD);*Parp1*$^{-/-}$ mBMCs. The absence of PARP1 strongly decreased the assembly of SMARCAD1 on chromatin and on DSBs (marked by γH2AX) (Figure 6C and D, respectively). Immunofluorescence staining revealed inhibition of colocalization of PARP1 and SMARCAD1 in FLT3(ITD);*Dnmt3a*^{KD} 32Dcl3 cells when compared to FLT3(ITD) counterparts (Figure 6E), further supporting the role of PARP1 as an anchor of SMARCAD1 on DSBs in leukemia cells.

Therefore, we tested the role of repressive PARP1-SMARCAD1-MSH2/MSH3 pathway in enhanced assembly of Polθ on DNA damage and limited DNA end resection in FLT3(ITD);*Dnmt3a*^{KD} 32Dcl3 cells. Remarkably, while expression of SMARCAD1, MSH2 and MHS3 proteins were similar in total cell lysates, a severe decrease of chromatin-bound SMARCAD1, MSH2 and MHS3 proteins was detected in irradiated FLT3(ITD);*Dnmt3a*^{KD} 32Dcl3 cells when compared to FLT3(ITD) counterparts (Figure 6F). Moreover, immunofluorescent staining showed strong reduction of SMARCAD1 assembly on DSBs (marked by γH2AX foci), and abrogation of SMARCAD1-MSH3 and MSH2/MSH3 colocalization in FLT3(ITD);*Dnmt3a*^{KD} cells when compared to FLT3(ITD) counterparts (Figure 6G-I, respectively). In addition, downregulation of MSH2 in FLT3(ITD) 32Dcl3 cells (Figure 6J, left panel) was also associated with enhanced formation of Polθ nuclear foci (Figure 6J, middle and right panels). In concordance, SMART assay (Figure 6K, left panel) revealed decreased DNA end processing in FLT3(ITD) cells with MSH2 knockdown when compared to FLT3(ITD) counterparts (Figure 6K, right panel).

It has been also reported that SMARCAD1 preferentially associates with H3 citrullinated on arginine 26 (H3R26Cit) (81). However, DNMT3A deficiency was not associated with any changes in H3R26Cit levels (Supplemental Figure S6B), highlighting the role of PARP1, but not H3R26Cit in SMARCAD1 recruitment to DSBs in leukemia cells.

Activation of PLK1 kinase [phosphorylates RHINO1 and Polθ to stimulate TMEJ in mitosis (82)] assessed by phosphorylation on Thr210 (83) and expression of RHINO [interacts with Polθ enabling its recruitment to DSBs during mitosis (84)] were upregulated by DNMT3A knockdown (Supplemental Figure S6C), and may enhance Polθ recruitment to DNA damage sites in mitosis. However, there was no significant differences in G2/M cell cycle phase and sensitivity to PLK1 inhibitor between FLT3(ITD);*Dnmt3a*^{KD} and FLT3(ITD) 32Dcl3 cells (Supplemental Figure S6D and E, respectively), arguing against a major role of PLK1-RHINO axis in Polθ recruitment to DSBs and activation of TMEJ in DNMT3A deficient leukemia cells.

Altogether, we postulate that inhibition of the assembly of repressive PARP1-SMARCAD1-MSH2/MSH3 complex, but not facilitation of PLK1-RHINO axis or H3R26Cit, is a major stimulator of enhanced recruitment of Polθ to DNA damage sites in FLT3(ITD);*Dnmt3a*^{KD} cells (Figure 6L). This effect resulted in limited DNA end resection, stimulation of TMEJ and hypersensitivity to Polθ inhibition.

Standard drugs enhanced the effect of Polθ inhibitors against *DNMT3A*-mutated AML.

Polθ plays a key role in DNMT3A deficient leukemias, therefore we tested the potential therapeutic value of targeting Polθ. Inhibition of Polθ was synthetic lethal in cells with *BRCA1/2* mutations (68,69). Since FLT3 kinase inhibitor (FLT3i) induced acute BRCA1/2 deficiency in FLT3(ITD)-positive AML cells (36), we hypothesized that it would also sensitize FLT3(ITD)-positive DNMT3A deficient cells to Polθ inhibitors. Thus, the combinations of FLT3i quizartinib and Polθi ART558 or ART812 were tested against FLT3(ITD);*Dnmt3a*^{KD} 32Dcl3 cells and Lin^{-}CD34^{+} FLT3(ITD);DNMT3A(R882H) AML primary cells characterized before (22). In concordance, we show that quizartinib when combined with ART558 or ART812 eradicated FLT3(ITD);*Dnmt3a*^{KD} 32Dcl3 clonogenic cells *in vitro* and exerted >500 times stronger effect against Lin^{-}CD34^{+} FLT3(ITD);DNMT3A(R882H) AML cells when compared to individual

treatments (Figure 7A). Lin$^-$CD34$^+$ counterparts from healthy donors were not significantly affected by the treatment.

We also reported that the repair of etoposide-induced DNA-protein crosslinks (DPCs) is promoted by Polθ (58). We show here that the combination of sub-optimal concentrations of etoposide and Polθi ART558, ART812 or RP-6685 eradicated FLT3(ITD);*Dnmt3a*^{KD} 32Dcl3 clonogenic cells *in vitro* and exerted >12 times stronger effect against Lin$^-$CD34$^+$ FLT3(ITD);DNMT3A(R882H) AML cells when compared to individual treatments (Figure 7B). Again, Lin$^-$CD34$^+$ cells from healthy donors were not significantly affected.

Moreover, *DNMT3A* mutations sensitized AML cells to a replication stalling agent cytarabine (AraC) (30). Suboptimal concentrations of AraC combined with ART558 exerted 3x and 5x more potent effect against FLT3(ITD);*Dnmt3a*^{KD} 32Dcl3 cells and Lin$^-$CD34$^+$ FLT3(ITD);DNMT3A(R882H) AML cells, respectively, when compared to individual inhibitors (Figure 7C).

In addition, DNMT3A(R882H) AML cells were selectively susceptible to the hypomethylating agent azacytidine due to enhanced endogenous cell autonomous viral mimicry response (85). However, azacytidine did not substantially enhance the inhibitory effect of ART558 in FLT3(ITD);*Dnmt3a*^{KD} 32Dcl3 cells (Figure 7D).

Finally, we tested the effectiveness of Polθi RP-6685, a potent, selective, and orally bioavailable Polθi (48) alone and in combination with etoposide against very aggressive GFP+ FLT3(ITD);*Dnmt3a*^{KD} 32Dcl3 leukemia cells in NRG mice (MST 23.3± 0.3 days after i.v. injection of 10^3 cells). FLT3(ITD);*Dnmt3a*^{KD} 32Dcl3 leukemia cells already harbor numerous endogenous DPCs (Supplemental Figure S2C), and the combination of etoposide + RP-6685 was particularly effective in facilitating the accumulation of DPCs and toxic DSBs (Figure 7E and F, respectively). In concordance, treatment of GFP+ FLT3(ITD);*Dnmt3a*^{KD} 32Dcl3 leukemia – bearing mice with RP-6685 or etoposide (Figure 7G) diminished the percentage of GFP+

leukemia cells in peripheral blood by >2-fold. Remarkably, the combination of RP-6685 + etoposide reduced GFP+ cells below detectable levels in 6/7 mice (Figure 7H). The overall survival of leukemia mice treated with individual RP-6685 or etoposide was prolonged to 34.5±1.2 and 32.6±0.7 days, respectively whereas the combination of RP-6685 + etoposide extended the survival to 58.6±5.0 days (Figure 7I). No obvious toxicity was attributed to the treatment. In conclusion, addition of etoposide greatly enhanced anti-leukemia effect of Polθi *in vivo*.

Discussion

Accumulation of DNA damage and modulation of DDR are the hallmarks of cancer (86). DDR gene alterations are prevalent in many cancer types and led to development of novel therapeutic strategies, e.g., synthetic lethality triggered by PARP inhibitors in HR-deficient tumors including leukemia (15,31,87-89). *Ex vivo* drug sensitivity screens have been applied to identify additional targets for antitumor treatments (90). Using this strategy, we discovered unexpected vulnerability of *DNMT3A* mutated leukemia cells – their unique dependence on Polθ. This observation was corroborated by genetic and epigenetic analyses of the functional interdependence of DNMT3A and Polθ.

Remarkably, we found that Polθ was heavily overexpressed in DNMT3A-deficient leukemia cells, which depended on the process called PARylation-dependent ubiquitination (PARdU) (91). In PARdU the targeted protein is initially PARylated, which triggers an E3 ligase -mediated ubiquitination, resulting in proteasomal degradation of the protein. Here we determined that DNMT3A deficiency repressed PARP1-mediated PARdU of Polθ by the UBE2O E3 ligase, resulting in protection of Polθ from proteasomal degradation.

We also showed that DNMT3A deficiency not only enhanced Polθ expression, but also modulated processing of the DNA damage sites to favor Polθ-mediated TMEJ and fork restart in leukemia cells. DNMT3A deficient leukemia cells displayed limited DNA end resection due to dysregulation of the assembly of PARP1-SMARCAD1-MSH2/MSH3 repressive complex, which in turn facilitated Polθ recruitment to DNA damage sites and promoted TMEJ. This conclusion is supported by the reports that the absence of SMARCAD1 promoted TMEJ (80). Moreover, SMARCAD1 deficiency caused frequent fork stalling/inefficient fork restart, which require Polθ to restart the forks [(92) and this work]. These two Polθ-mediated activities, TMEJ and replication fork restart, are most likely required to counteract genotoxic effect of excessive formaldehyde-

induced DPCs-triggered DSBs and stressed replication forks in DNMT3A deficient leukemia cells (26,57,58,93).

It has been reported that survival of HR-deficient cells under genotoxic stress depends on Polθ-mediated DNA repair (69). Although DNMT3A-deficient leukemia cells did not display any detectable changes in the expression of HR proteins and in HR activity measured by extrachromosomal reporter cassette (22), diminished RPA and RAD51 foci formation and limited DNA end resection revealed a potential competition between Polθ-mediated TMEJ and RAD51-mediated HR in these cells. This unexpected observation is supported by the report of crosstalk between HR and Polθ in S phase (82). Polθ recruitment to DSBs to facilitate TMEJ in S phase is reliant on HR intermediates whereby Polθ appears to displace RAD51, a key HR factor, from ssDNA and may also counteract RPA, another HR factor (25,69,82,94,95). Thus, the abundance of Polθ in DNMT3A-deficient leukemia cells might facilitate the eviction of RAD51 and/or RPA from DSBs to promote TMEJ (68).

The interplay between downregulated PARP1 and upregulated Polθ appears unique for *DNMT3A* mutated leukemia cells. For example, inactivating mutations in *TET2* gene [encodes methylcytosine dioxygenase 2 that catalyzes the conversion of methylcytosine to 5-hydroxymethylcytosine, (10,13,96)] exert an opposite effect on PARP1 and Polθ expression, TMEJ and fork restarting activities, and sensitivity to Polθ inhibition. Polθ was barely detectable in TET2 deficient leukemia cells coinciding with low TMEJ activity, lack of the impact on fork restart and resistance to Polθ inhibitors. Thus, it appears that the sensitivity of leukemia cells to Polθi was associated with the expression levels of Polθ; DNMT3A deficient cells - the highest expressors - were hypersensitive, whereas TET2 deficient cells - the lowest expressors - were resistant. This observation is in concordance with reports implicating high expression of Polθ with sensitivity to the inhibitors (51,52).

To date, there are no reported human cancers with defects in the TMEJ, thus *TET2* mutated malignancy is the first one identified with TMEJ deficiency. We reported that *TET2* mutated leukemia cells are also HR deficient, thus the double deficiency in TMEJ and HR explain enhanced sensitivity to PARP and DNA-PKcs inhibitors [(22) and this work].

It should be noted that *DNMT3A* mutations are accompanied by other mutations (10,13,96), which might affect the response of leukemia clones to DDR inhibitors, including Polθi (16,22,36,50,97). For example, Polθi were very efficient in eliminating primary AML cells bearing FLT3(ITD);*DNMT3Amut* especially in combination with FLT3 kinase inhibitor quizartinib and topoisomerase II inhibitor etoposide. Quizartinib most likely hypersensitized FLT3(ITD);*DNMT3Amut* cells to Polθi due to induction of HR and D-NHEJ deficiencies (36). Similar effect would be expected in JAK2(V617F);*DNMT3Amut* MPN cells treated with JAK1/2 kinase inhibitor ruxolitinib (16). On the other hand, the beneficial effect of etoposide and Polθi could depend on accumulation of DPC-mediated toxic DSBs (18,58). Cytarabine also enhanced the effect of Polθi in FLT3(ITD);*DNMT3Amut* cells, most likely due to a cumulative effect of cytarabine-mediated fork collapse (30) and Polθi-mediated delay of replication fork restart (this work). However, azacytidine which selectively suppressed protein translation and induced apoptosis in *DNMT3Amut* cells via viral mimicry response (85) only modestly enhanced the effect of Polθi. Therefore, it is paramount to determine if/how additional clinically relevant mutations may affect the sensitivity of *DNMT3A* mutated leukemia cells to Polθi +/- standard drugs.

Altogether, we postulate that acquisition of DNMT3A deficiency in leukemia cells triggered the negative feedback loop between PARP1 and Polθ to promote abundant expression of Polθ and restrict DNA end resection, resulting in hyperactive TMEJ, fork restarting and hypersensitivity to Polθ inhibition (Supplemental Figure S7). Somatic *DNMT3A* mutations are frequent in myeloid malignancies [for example in 23-37% of cytogenetically normal AML

(98)], thus the unique dependence of *DNMT3A*-mutated malignancies on Polθ could be exploited therapeutically by applying Polθi alone and in combination with pre-selected standard modalities. However, since DNMT3A deficiency has been also reported in different types of solid tumors (e.g., lung and colon cancers, melanoma), pharmacological targeting of Polθ may have more broad application (2-4). This possibility is highlighted by recent clinical trials testing Polθ inhibitors against solid tumors (NCT05687110, NCT05898399, NCT04991480). Since inhibition of Polθ triggered cGAS/STING pathway [(99) and this work], stimulation of immune response may also contribute to anti-tumor effect of Polθi (100).

Authors contribution

BVL, UV, MMT, MN-S, M-CC, MG, ZH, MW, JG, EV-W, PP-B, A-MK, SZ and GC performed investigation and formal analysis. EH and PV performed forma analysis and provided AML patient samples, KP supervised PP-B, RP supervised GC, GSV and BJP supervised MG, AB supervised MW, and J-YM supervised M-CC. GPG and GAC contributed to investigation. TS conceptualized the idea, acquired funding, supervised BVL, UV, MMT, MN-S, and ZH, and wrote the manuscript.

Acknowledgements

This work was supported by R01CA186238, R01CA237286, R01CA244044, R01CA244179, R01CA247707, R01CA283396 and LLS TRP 6628-21 to T.S. G.A.C was supported by the National Institutes of Health R01DK124883 and the Leukemia and Lymphoma Society (6667-23). G.P.G was supported by P01CA247773. G.S.V. and B.J.P.H. were supported by the Bloodwise Program Grant (17006) and Blood Cancer UK Grant (21006). JYM is a Canada Research Chair in DNA repair and Cancer Therapeutics and was supported by a CIHR Foundation grant (IC118540). P.P-B. was supported by the grant 2018/30/M/NZ3/00274 from

the National Science Center, Poland. We thank Dr. Sara H. Small (Fox Chase Cancer Center and Fels Cancer Institute for Personalized Medicine) for critical reading of the manuscript. We acknowledge Boris Bartholdy from Albert Einstein College of Medicine, Bronx, NY, USA for his involvement in analyzing PARP1 methylation and expression in the published database. We also thank Pedro Torres-Ayuso and Dr. Oneida Arosarena (Temple University, Lewis Katz School of Medicine) for kindly providing non-small cell lung cancer cell lines for our research.

References

1. Sato H, Wheat JC, Steidl U, Ito K. DNMT3A and TET2 in the Pre-Leukemic Phase of Hematopoietic Disorders. Front Oncol **2016**;6:187
2. Zhang J, Yang C, Wu C, Cui W, Wang L. DNA Methyltransferases in Cancer: Biology, Paradox, Aberrations, and Targeted Therapy. Cancers **2020**;12
3. Kim MS, Kim YR, Yoo NJ, Lee SH. Mutational analysis of DNMT3A gene in acute leukemias and common solid cancers. Apmis **2013**;121:85-94
4. AACR. AACR Project GENIE: Powering Precision Medicine through an International Consortium. Cancer discovery **2017**;7:818-31
5. Okano M, Bell DW, Haber DA, Li E. DNA methyltransferases Dnmt3a and Dnmt3b are essential for de novo methylation and mammalian development. Cell **1999**;99:247-57. doi: 10.1016/s0092-8674(00)81656-6.
6. Guryanova OA, Shank K, Spitzer B, Luciani L, Koche RP, Garrett-Bakelman FE*, et al.* DNMT3A mutations promote anthracycline resistance in acute myeloid leukemia via impaired nucleosome remodeling. Nat Med **2016**;22:1488-95
7. Knudsen TA, Skov V, Stevenson K, Werner L, Duke W, Laurore C*, et al.* Genomic profiling of a randomized trial of interferon-α vs hydroxyurea in MPN reveals mutation-specific responses. Blood advances **2022**;6:2107-19
8. Nteliopoulos G, Bazeos A, Claudiani S, Gerrard G, Curry E, Szydlo R*, et al.* Somatic variants in epigenetic modifiers can predict failure of response to imatinib but not to second-generation tyrosine kinase inhibitors. Haematologica **2019**;104:2400-9
9. Mohanty V, Baran N, Huang Y, Ramage CL, Cooper LM, He S*, et al.* Transcriptional and phenotypic heterogeneity underpinning venetoclax resistance in AML. bioRxiv **2024**
10. Ley TJ, Miller C, Ding L, Raphael BJ, Mungall AJ, Robertson A*, et al.* Genomic and epigenomic landscapes of adult de novo acute myeloid leukemia. The New England journal of medicine **2013**;368:2059-74
11. Liang S, Zhou X, Pan H, Yang Y, Shi L, Wang L. Prognostic value of DNMT3A mutations in myelodysplastic syndromes: a meta-analysis. Hematology **2019**;24:613-22
12. Nangalia J, Nice FL, Wedge DC, Godfrey AL, Grinfeld J, Thakker C*, et al.* DNMT3A mutations occur early or late in patients with myeloproliferative neoplasms and mutation order influences phenotype. Haematologica **2015**;100:e438-42
13. Rinke J, Hochhaus A, Ernst T. CML - Not only BCR-ABL1 matters. Best Pract Res Clin Haematol **2020**;33:101194
14. Klco JM, Miller CA, Griffith M, Petti A, Spencer DH, Ketkar-Kulkarni S*, et al.* Association Between Mutation Clearance After Induction Therapy and Outcomes in Acute Myeloid Leukemia. JAMA **2015**;314:811-22
15. Esposito MT, So CW. DNA damage accumulation and repair defects in acute myeloid leukemia: implications for pathogenesis, disease progression, and chemotherapy resistance. Chromosoma **2014**;123:545-61
16. Nieborowska-Skorska M, Maifrede S, Dasgupta Y, Sullivan K, Flis S, Le BV*, et al.* Ruxolitinib-induced defects in DNA repair cause sensitivity to PARP inhibitors in myeloproliferative neoplasms. Blood **2017**;130:2848-59

17. Chen E, Ahn JS, Massie CE, Clynes D, Godfrey AL, Li J*, et al.* JAK2V617F promotes replication fork stalling with disease-restricted impairment of the intra-S checkpoint response. Proceedings of the National Academy of Sciences of the United States of America **2014**;111:15190-5

18. Vekariya U, Toma M, Nieborowska-Skorska M, Le BV, Caron MC, Kukuyan AM*, et al.* DNA polymerase theta protects leukemia cells from metabolically induced DNA damage. Blood **2023**;141:2372-89

19. Jackson SP. Sensing and repairing DNA double-strand breaks. Carcinogenesis **2002**;23:687-96.

20. Le BV, Podszywałow-Bartnicka P, Piwocka K, Skorski T. Pre-Existing and Acquired Resistance to PARP Inhibitor-Induced Synthetic Lethality. Cancers **2022**;14

21. Ray Chaudhuri A, Nussenzweig A. The multifaceted roles of PARP1 in DNA repair and chromatin remodelling. Nature reviews Molecular cell biology **2017**;18:610-21

22. Maifrede S, Le BV, Nieborowska-Skorska M, Golovine K, Sullivan-Reed K, Dunuwille WMB*, et al.* TET2 and DNMT3A Mutations Exert Divergent Effects on DNA Repair and Sensitivity of Leukemia Cells to PARP Inhibitors. Cancer research **2021**;81:5089-101

23. Ramsden DA, Carvajal-Garcia J, Gupta GP. Mechanism, cellular functions and cancer roles of polymerase-theta-mediated DNA end joining. Nature reviews Molecular cell biology **2021**

24. Fijen C, Drogalis Beckham L, Terino D, Li Y, Ramsden DA, Wood RD*, et al.* Sequential requirements for distinct Polθ domains during theta-mediated end joining. Molecular cell **2024**;84:1460-74.e6

25. Wyatt DW, Feng W, Conlin MP, Yousefzadeh MJ, Roberts SA, Mieczkowski P*, et al.* Essential Roles for Polymerase theta-Mediated End Joining in the Repair of Chromosome Breaks. Molecular cell **2016**;63:662-73

26. Wang Z, Song Y, Li S, Kurian S, Xiang R, Chiba T*, et al.* DNA polymerase theta (POLQ) is important for repair of DNA double-strand breaks caused by fork collapse. J Biol Chem **2019**;294:3909-19. doi: 10.1074/jbc.RA118.005188. Epub 2019 Jan 17.

27. Schrempf A, Bernardo S, Arasa Verge EA, Ramirez Otero MA, Wilson J, Kirchhofer D*, et al.* POLθ processes ssDNA gaps and promotes replication fork progression in BRCA1-deficient cells. Cell reports **2022**;41:111716

28. Mann A, Ramirez-Otero MA, De Antoni A, Hanthi YW, Sannino V, Baldi G*, et al.* POLθ prevents MRE11-NBS1-CtIP-dependent fork breakage in the absence of BRCA2/RAD51 by filling lagging-strand gaps. Molecular cell **2022**;82:4218-31.e8

29. Belan O, Sebald M, Adamowicz M, Anand R, Vancevska A, Neves J*, et al.* POLQ seals post-replicative ssDNA gaps to maintain genome stability in BRCA-deficient cancer cells. Molecular cell **2022**;82:4664-80.e9

30. Venugopal K, Feng Y, Nowialis P, Xu H, Shabashvili DE, Berntsen CM*, et al.* DNMT3A Harboring Leukemia-Associated Mutations Directs Sensitivity to DNA Damage at Replication Forks. Clinical cancer research : an official journal of the American Association for Cancer Research **2022**;28:756-69

31. Nieborowska-Skorska M, Sullivan K, Dasgupta Y, Podszywalow-Bartnicka P, Hoser G, Maifrede S*, et al.* Gene expression and mutation-guided synthetic lethality eradicates proliferating and quiescent leukemia cells. J Clin Invest **2017**;127:2392-406

32. Quentmeier H, MacLeod RA, Zaborski M, Drexler HG. JAK2 V617F tyrosine kinase mutation in cell lines derived from myeloproliferative disorders. Leukemia **2006**;20:471-6

33. Quentmeier H, Pommerenke C, Dirks WG, Fähnrich S, Hauer V, Uphoff CC*, et al.* DNMT3A R882H mutation in acute myeloid leukemia cell line SET-2. Leukemia research **2020**;88:106270

34. Lee BH, Tothova Z, Levine RL, Anderson K, Buza-Vidas N, Cullen DE*, et al.* FLT3 mutations confer enhanced proliferation and survival properties to multipotent progenitors in a murine model of chronic myelomonocytic leukemia. Cancer cell **2007**;12:367-80

35. Kuhn R, Schwenk F, Aguet M, Rajewsky K. Inducible gene targeting in mice. Science **1995**;269:1427-9

36. Maifrede S, Nieborowska-Skorska M, Sullivan-Reed K, Dasgupta Y, Podszywalow-Bartnicka P, Le BV*, et al.* Tyrosine kinase inhibitor-induced defects in DNA repair sensitize FLT3(ITD)-positive leukemia cells to PARP1 inhibitors. Blood **2018**;132:67-77

37. Huang F, Goyal N, Sullivan K, Hanamshet K, Patel M, Mazina OM*, et al.* Targeting BRCA1- and BRCA2-deficient cells with RAD52 small molecule inhibitors. Nucleic acids research **2016**;44:4189-99

38. Fried W, Tyagi M, Minakhin L, Chandramouly G, Tredinnick T, Ramanjulu M*, et al.* Discovery of a small-molecule inhibitor that traps Polθ on DNA and synergizes with PARP inhibitors. Nature communications **2024**;15:2862

39. Huang S, Stillson NJ, Sandoval JE, Yung C, Reich NO. A novel class of selective non-nucleoside inhibitors of human DNA methyltransferase 3A. Bioorg Med Chem Lett **2021**;40:127908

40. Cramer-Morales K, Nieborowska-Skorska M, Scheibner K, Padget M, Irvine DA, Sliwinski T*, et al.* Personalized synthetic lethality induced by targeting RAD52 in leukemias identified by gene mutation and expression profile. Blood **2013**;122:1293-304

41. Vekariya U, Rawat K, Saxena R, Tripathi RK. Identification of MΦ specific POTEE expression: Its role in mTORC2 activation via protein-protein interaction in TAMs. Cell Immunol **2019**;335:30-40

42. Vekariya U, Saxena R, Singh P, Rawat K, Kumar B, Kumari S*, et al.* HIV-1 Nef-POTEE; A novel interaction modulates macrophage dissemination via mTORC2 signaling pathway. Life Sci **2018**;214:158-66

43. Feng W, Simpson DA, Cho JE, Carvajal-Garcia J, Smith CM, Headley KM*, et al.* Marker-free quantification of repair pathway utilization at Cas9-induced double-strand breaks. Nucleic acids research **2021**;49:5095-105

44. O'Sullivan J, Mersaoui SY, Poirier G, Masson JY. Assessment of Global DNA Double-Strand End Resection using BrdU-DNA Labeling coupled with Cell Cycle Discrimination Imaging. Journal of visualized experiments : JoVE **2021**

45. Bryant HE, Petermann E, Schultz N, Jemth AS, Loseva O, Issaeva N*, et al.* PARP is activated at stalled forks to mediate Mre11-dependent replication restart and recombination. EMBO J **2009**;28:2601-15

46. Panzarino NJ, Krais JJ, Cong K, Peng M, Mosqueda M, Nayak SU*, et al.* Replication Gaps Underlie BRCA Deficiency and Therapy Response. Cancer research **2021**;81:1388-97

47. Altieri A, Dell'Aquila M, Pentimalli F, Giordano A, Alfano L. SMART (Single Molecule Analysis of Resection Tracks) Technique for Assessing DNA end-Resection in Response to DNA Damage. Bio Protoc **2020**;10:e3701

48. Bubenik M, Mader P, Mochirian P, Vallée F, Clark J, Truchon JF*, et al.* Identification of RP-6685, an Orally Bioavailable Compound that Inhibits the DNA Polymerase Activity of Polθ. Journal of medicinal chemistry **2022**;65:13198-215

49. Cheema TA, Kanai R, Kim GW, Wakimoto H, Passer B, Rabkin SD*, et al.* Enhanced antitumor efficacy of low-dose Etoposide with oncolytic herpes simplex virus in human glioblastoma stem cell xenografts. Clinical cancer research : an official journal of the American Association for Cancer Research **2011**;17:7383-93

50. Toma MM, Karami A, Nieborowska-Skorska M, Chirtala KN, Pepek M, Hadzijusufovic E*, et al.* Clonal medicine targeting DNA damage response eradicates leukemia. Leukemia **2024**

51. Zatreanu D, Robinson HMR, Alkhatib O, Boursier M, Finch H, Geo L*, et al.* Polθ inhibitors elicit BRCA-gene synthetic lethality and target PARP inhibitor resistance. Nature communications **2021**;12:3636

52. Zhou J, Gelot C, Pantelidou C, Li A, Yücel H, Davis RE*, et al.* A first-in-class polymerase theta inhibitor selectively targets homologous-recombination-deficient tumors. Nature Cancer **2021**;2:598-610

53. Stockley ML, Ferdinand A, Benedetti G, Blencowe P, Boyd SM, Calder M*, et al.* Discovery, Characterization, and Structure-Based Optimization of Small-Molecule In Vitro and In Vivo Probes for Human DNA Polymerase Theta. Journal of medicinal chemistry **2022**;65:13879-91

54. Zheng W, Liu A, Xia N, Chen N, Meurens F, Zhu J. How the Innate Immune DNA Sensing cGAS-STING Pathway Is Involved in Apoptosis. Int J Mol Sci **2023**;24

55. Haag SM, Gulen MF, Reymond L, Gibelin A, Abrami L, Decout A*, et al.* Targeting STING with covalent small-molecule inhibitors. Nature **2018**;559:269-73

56. Nieborowska-Skorska M, Kopinski PK, Ray R, Hoser G, Ngaba D, Flis S*, et al.* Rac2-MRC-cIII-generated ROS cause genomic instability in chronic myeloid leukemia stem cells and primitive progenitors. Blood **2012**;119:4253-63

57. Stingele J, Bellelli R, Boulton SJ. Mechanisms of DNA-protein crosslink repair. Nature reviews Molecular cell biology **2017**;18:563-73

58. Chandramouly G, Liao S, Rusanov T, Borisonnik N, Calbert ML, Kent T*, et al.* Polθ promotes the repair of 5'-DNA-protein crosslinks by microhomology-mediated end-joining. Cell reports **2021**;34:108820

59. Yousefzadeh MJ, Wyatt DW, Takata K, Mu Y, Hensley SC, Tomida J*, et al.* Mechanism of suppression of chromosomal instability by DNA polymerase POLQ. PLoS genetics **2014**;10:e1004654

60. Garzon G, Gomez S, Mantilla D, Martinez F. A deep CT to MRI unpaired translation that preserve ischemic stroke lesions. Annu Int Conf IEEE Eng Med Biol Soc **2022**;2022:2708-11

61. De Vos M, El Ramy R, Quénet D, Wolf P, Spada F, Magroun N*, et al.* Poly(ADP-ribose) polymerase 1 (PARP1) associates with E3 ubiquitin-protein ligase UHRF1 and

modulates UHRF1 biological functions. The Journal of biological chemistry **2014**;289:16223-38

62. Gatti M, Imhof R, Huang Q, Baudis M, Altmeyer M. The Ubiquitin Ligase TRIP12 Limits PARP1 Trapping and Constrains PARP Inhibitor Efficiency. Cell reports **2020**;32:107985

63. Zhang N, Zhang Y, Qian H, Wu S, Cao L, Sun Y. Selective targeting of ubiquitination and degradation of PARP1 by E3 ubiquitin ligase WWP2 regulates isoproterenol-induced cardiac remodeling. Cell Death Differ **2020**;27:2605-19

64. Coll-Martínez B, Crosas B. How the 26S Proteasome Degrades Ubiquitinated Proteins in the Cell. Biomolecules **2019**;9

65. Lopes UG, Erhardt P, Yao R, Cooper GM. p53-dependent induction of apoptosis by proteasome inhibitors. The Journal of biological chemistry **1997**;272:12893-6

66. Vekariya U, Minakhin L, Chandramouly G, Tyagi M, Kent T, Sullivan-Reed K*, et al.* PARG is essential for Polθ-mediated DNA end-joining by removing repressive poly-ADP-ribose marks. Nature communications **2024**;15:5822

67. Kais Z, Rondinelli B, Holmes A, O'Leary C, Kozono D, D'Andrea AD*, et al.* FANCD2 Maintains Fork Stability in BRCA1/2-Deficient Tumors and Promotes Alternative End-Joining DNA Repair. Cell reports **2016**;15:2488-99

68. Mateos-Gomez PA, Gong F, Nair N, Miller KM, Lazzerini-Denchi E, Sfeir A. Mammalian polymerase theta promotes alternative NHEJ and suppresses recombination. Nature **2015**;518:254-7

69. Ceccaldi R, Liu JC, Amunugama R, Hajdu I, Primack B, Petalcorin MI*, et al.* Homologous-recombination-deficient tumours are dependent on Poltheta-mediated repair. Nature **2015**;518:258-62

70. Setiaputra D, Durocher D. Shieldin - the protector of DNA ends. EMBO Rep **2019**;20

71. Zhao F, Kim W, Kloeber JA, Lou Z. DNA end resection and its role in DNA replication and DSB repair choice in mammalian cells. Exp Mol Med **2020**;52:1705-14

72. van de Kamp G, Heemskerk T, Kanaar R, Essers J. DNA Double Strand Break Repair Pathways in Response to Different Types of Ionizing Radiation. Front Genet **2021**;12:738230

73. Cruz-García A, López-Saavedra A, Huertas P. BRCA1 accelerates CtIP-mediated DNA-end resection. Cell reports **2014**;9:451-9

74. Sartori AA, Lukas C, Coates J, Mistrik M, Fu S, Bartek J*, et al.* Human CtIP promotes DNA end resection. Nature **2007**;450:509-14

75. Graeser M, McCarthy A, Lord CJ, Savage K, Hills M, Salter J*, et al.* A marker of homologous recombination predicts pathologic complete response to neoadjuvant chemotherapy in primary breast cancer. Clinical cancer research : an official journal of the American Association for Cancer Research **2010**;16:6159-68

76. Luedeman ME, Stroik S, Feng W, Luthman AJ, Gupta GP, Ramsden DA. Poly(ADP) ribose polymerase promotes DNA polymerase theta-mediated end joining by activation of end resection. Nature communications **2022**;13:4547

77. Caron MC, Sharma AK, O'Sullivan J, Myler LR, Ferreira MT, Rodrigue A*, et al.* Poly(ADP-ribose) polymerase-1 antagonizes DNA resection at double-strand breaks. Nature communications **2019**;10:2954

78. Xu G, Chapman JR, Brandsma I, Yuan J, Mistrik M, Bouwman P*, et al.* REV7 counteracts DNA double-strand break resection and affects PARP inhibition. Nature **2015**;521:541-4

79. Rowbotham SP, Barki L, Neves-Costa A, Santos F, Dean W, Hawkes N*, et al.* Maintenance of silent chromatin through replication requires SWI/SNF-like chromatin remodeler SMARCAD1. Molecular cell **2011**;42:285-96

80. Oh JM, Kang Y, Park J, Sung Y, Kim D, Seo Y*, et al.* MSH2-MSH3 promotes DNA end resection during homologous recombination and blocks polymerase theta-mediated end-joining through interaction with SMARCAD1 and EXO1. Nucleic acids research **2023**;51:5584-602

81. Xiao S, Lu J, Sridhar B, Cao X, Yu P, Zhao T*, et al.* SMARCAD1 Contributes to the Regulation of Naive Pluripotency by Interacting with Histone Citrullination. Cell reports **2017**;18:3117-28

82. Gelot C, Kovacs MT, Miron S, Mylne E, Haan A, Boeffard-Dosierre L*, et al.* Polθ is phosphorylated by PLK1 to repair double-strand breaks in mitosis. Nature **2023**;621:415-22

83. Tavernier N, Thomas Y, Vigneron S, Maisonneuve P, Orlicky S, Mader P*, et al.* Bora phosphorylation substitutes in trans for T-loop phosphorylation in Aurora A to promote mitotic entry. Nature communications **2021**;12:1899

84. Brambati A, Sacco O, Porcella S, Heyza J, Kareh M, Schmidt JC*, et al.* RHINO directs MMEJ to repair DNA breaks in mitosis. Science **2023**:eadh3694

85. Scheller M, Ludwig AK, Göllner S, Rohde C, Krämer S, Stäble S*, et al.* Hotspot DNMT3A mutations in clonal hematopoiesis and acute myeloid leukemia sensitize cells to azacytidine via viral mimicry response. Nat Cancer **2021**;2:527-44

86. Hanahan D. Hallmarks of Cancer: New Dimensions. Cancer discovery **2022**;12:31-46

87. Murai J, Pommier Y. BRCAness, Homologous Recombination Deficiencies, and Synthetic Lethality. Cancer research **2023**;83:1173-4

88. Knijnenburg TA, Wang L, Zimmermann MT, Chambwe N, Gao GF, Cherniack AD*, et al.* Genomic and Molecular Landscape of DNA Damage Repair Deficiency across The Cancer Genome Atlas. Cell Rep **2018**;23:239-54.e6. doi: 10.1016/j.celrep.2018.03.076.

89. Kontandreopoulou CN, Diamantopoulos PT, Tiblalexi D, Giannakopoulou N, Viniou NA. PARP1 as a therapeutic target in acute myeloid leukemia and myelodysplastic syndrome. Blood advances **2021**;5:4794-805

90. Kitaeva KV, Rutland CS, Rizvanov AA, Solovyeva VV. Cell Culture Based in vitro Test Systems for Anticancer Drug Screening. Front Bioeng Biotechnol **2020**;8:322

91. Vivelo CA, Ayyappan V, Leung AKL. Poly(ADP-ribose)-dependent ubiquitination and its clinical implications. Biochem Pharmacol **2019**;167:3-12

92. Lo CSY, van Toorn M, Gaggioli V, Paes Dias M, Zhu Y, Manolika EM*, et al.* SMARCAD1-mediated active replication fork stability maintains genome integrity. Sci Adv **2021**;7

93. Mórocz M, Zsigmond E, Tóth R, Enyedi MZ, Pintér L, Haracska L. DNA-dependent protease activity of human Spartan facilitates replication of DNA-protein crosslink-containing DNA. Nucleic acids research **2017**;45:3172-88

94. Mateos-Gomez PA, Kent T, Deng SK, McDevitt S, Kashkina E, Hoang TM*, et al.* The helicase domain of Polθ counteracts RPA to promote alt-NHEJ. Nature structural & molecular biology **2017**;24:1116-23

95. Schaub JM, Soniat MM, Finkelstein IJ. Polymerase theta-helicase promotes end joining by stripping single-stranded DNA-binding proteins and bridging DNA ends. Nucleic acids research **2022**

96. Maslah N, Benajiba L, Giraudier S, Kiladjian J-J, Cassinat B. Clonal architecture evolution in Myeloproliferative Neoplasms: from a driver mutation to a complex heterogeneous mutational and phenotypic landscape. Leukemia **2023**;37:957-63

97. Nieborowska-Skorska M, Paietta EM, Levine RL, Fernandez HF, Tallman MS, Litzow MR*, et al.* Inhibition of the mutated c-KIT kinase in AML1-ETO-positive leukemia cells restores sensitivity to PARP inhibitor. Blood advances **2019**;3:4050-4

98. Chen X, Tian C, Hao Z, Pan L, Hong M, Wei W*, et al.* The impact of DNMT3A variant allele frequency and two different comutations on patients with de novo cytogenetically normal acute myeloid leukemia. Cancer Med **2023**;12:10340-50

99. Oh G, Wang A, Wang L, Li J, Werba G, Weissinger D*, et al.* POLQ inhibition elicits an immune response in homologous recombination-deficient pancreatic adenocarcinoma via cGAS/STING signaling. J Clin Invest **2023**;133

100. Zhang J, Yu S, Peng Q, Wang P, Fang L. Emerging mechanisms and implications of cGAS-STING signaling in cancer immunotherapy strategies. Cancer Biol Med **2024**;21:45-64

Figure 1. Inactivation of DNMT3A selectively hypersensitized leukemia cells to Polθi. (**A**) A diagram illustrating DSB repair pathways. HR = homologous recombination, TA-HR = transcription associated HR, SSA = single strand annealing, NHEJ = non-homologous end-joining, TMEJ = Polθ-mediated end-joining. Proteins highlighted in red were targeted with small molecule inhibitors. Inset: a representative accumulation of γH2AX foci (DSBs) in leukemia cells. (**B**) FLT3(ITD)-positive 32Dcl3 cells (F) and isogenic cells lacking DNMT3A [FLT3(ITD);*Dnmt3a*^{KD} = FD) or TET2 (FLT3(ITD);*Tet2*^{KD} = FT] were treated with doxorubicin and the indicated inhibitors. Results represent mean % of colonies relative to untreated control. (**C**) Polθ inhibitors tested here; Hel = helicase domain, Pol = DNA polymerase domain. (**D-H**) F, FD ad FT 32Dcl3 cells (**D**), *Flt3*$^{ITD/ITD}$, *Flt3*$^{ITD//ITD}$;*Dnmt3a*$^{-/-}$ and *Flt3*$^{ITD/ITD}$;*Tet2*$^{-/-}$ Lin^{-}cKit^{+} mBMCs (**E**), Lin^{-}CD34^{+} AML patient cells (n=3 of each) carrying FLT3(ITD), FLT3(ITD);*DNMT3A*^{mut} and FLT3(ITD);*TET2*^{mut} (**F**), JAK2(V617F) human HEL cells and JAK2(V617F);DNMT3A(R882H) human SET-2 cells (**G**), and *Flt3*$^{ITD/+}$ and *Flt3*$^{ITD/+}$;*Dnmt3a*$^{R882H/+}$ Lin^{-}cKit^{+} mBMCs (**H**) were treated with the indicated Polθ inhibitors. Results represent mean % of colonies relative to untreated control. (**I**) Mean number of colonies of F 32Dcl3 cells treated, or not, with 4 μM DNMT3A-IN-1 and/or 10 μM RT-6685. *Right panels*: Detection of DNMT3A-IN-1 -mediated inhibition of 5-mC. (**J**) F (green), FD (orange), and FT (blue) 32Dcl3 cells were untreated (-) or treated with 20 μM ART558 for 24 hrs. Results represent mean % of DNA in the tail. (**K**) FD 32Dcl3 cells were untreated or treated with 5 μM ART558, 0.5 μM C-176 and the combination. *Left panel:* Mean number of colonies. *Right panel*: Representative Western blot detecting phospho-TBK1 kinase, total TBK1 and β-actin (loading control). Error bars represent the SD; p values were determined using one-way Anova (**B**, **D**-**F**, **I**-left panel, **J** and **K**) and Student's t test (**G, H, I**-Right panel).

Figure 2. Detrimental effect of genetic inactivation of Polθ in DNMT3A deficient leukemia cells. (**A-C**) GFP^{+} Lin^{-}cKit^{+}GFP^{+} *Dnmt3a*$^{-/-}$ (D) and *Dnmt3a*$^{-/-}$;*Polq*$^{-/-}$ (DP) mBMCs expressing FLT3(ITD) (FD and FDP, respectively), JAK2(V617F) (JD and JDP, respectively) and BCR-ABL1 (BD and BDP, respectively) were examined to detect mean (**A**) colony number, (**B**) % of γH2AX-positive cells, and (**C**) % of GFP^{+} cells in PBL of transplanted mice (n=5-9 mice/group). (**D, E**) *Flt3*$^{ITD/+}$;*Dnmt3a*$^{R882H/+}$ Lin^{-}cKit^{+}RFP^{+} mBMCs transduced with Polθ wild-type (WT) and D2230A+Y2231A dominant-negative mutant (DNM) were tested to detect (**D**) mean colony number and (**E**) % of γH2AX-positive cells. (**F-H**) RFP^{+} FLT3(ITD);*Dnmt3a*^{KD} 32Dcl3 cells transduced with Polθ wild-type (WT) and D2230A+Y2231A dominant-negative mutant (DNM) were tested to measure mean (**F**) number of colonies *in vitro* (*Inset*- Western blot), (**G**) % of RFP^{+} cells in PBL of transplanted SCID mice (n=10 mice/group), and (**H**) survival of the transplanted mice. Error bars represent the SD; p values were determined using Student's t test (**A-G**); mice survival was evaluated using Kaplan-Meier LogRank test (**H**).

Figure 3. DNMT3A deficiency downregulates PARP1 PARylation-dependent UBE2O-mediated ubiquitination of Polθ to elevate Polθ expression in leukemia cells. (**A-E**) Representative Western blots of the indicated proteins in: (**A**) FLT3(ITD) (F), FLT3(ITD);*Tet2*^{KD} (FT) and FLT3(ITD);*Dnmt3a*^{KD} (FD) 32Dcl3 cells and in Lin^{-} mBMCs from *Flt3*$^{ITD/ITD}$ (F), *Flt3*$^{ITD+/-}$; *Dnmt3a*$^{R882H/+}$ (FD^{mut}), *Flt3*$^{ITD/ITD}$;*Dnmt3a*$^{-/-}$ (FD^{KO}) and FLT3(ITD);*Tet2*^{KD} (FT^{KO}) mBMCs; (**B**) F 32Dcl3 cells treated (+) or not (-) with DNMT3A-IN-1; (**C**) F 32Dcl3 cells transduced with scrambled or *Parp1* specific shRNA; (**D**) *FLT3*^{ITD};*Parp1*$^{-/-}$ and *FLT3*^{ITD};*Parp1*$^{+/+}$ mBMCs; (**E**) FD

32Dcl3 cells and the clones transduced with PARP1 cDNA expression construct (FD-PARP1 cl1 and cl2). (**F**) Western analysis of F and FD-PARP1 32Dcl3 cells treated with 0.5 μM PARP1i AZD5305 for 0, 5 10 and 20 min. (**G**) Detection of PARylated Polθ in anti-Polθ immunoprecipitates (IP-Polθ) and total cell lysates (Input) from F and FD 32Dcl3 cells. (**H**) Western analysis of F and FD-PARP1 32Dcl3 cells treated (+) or not (-) with proteasome inhibitor MG132. (**I**) Detection of Polθ in anti-Ub immunoprecipitates (IP-Ub) and total cell lysates (Input) from F and FD 32Dcl3 cells. (**J**) Co-immunoprecipitation of Polθ and UBE2O in anti-Polθ immunoprecipitates (IP-Polθ) from F, FD and FD+PARP1 32Dcl3 cells; total cell lysates (Input) are shown, too. (**K**) Western analysis of FD+PARP1 32Dcl3 cells transduced with scrambled or *Ube2o* siRNA. (**L**) Co-immunoprecipitation of Polθ and UBE2O in anti-Polθ immunoprecipitates (IP-Polθ) from F and FD+PARP1 32Dcl3 cells treated (+) or not (-) with 0.5 μM AZD5305 for 60 min; total cell lysates (Input) are shown, too. Mean ± SD and statistical significance of the intensity of specific proteins/protein posttranslational modifications are shown. p values were determined using one-way Anova (**A**, **C, E, F, H, J**) and Student's t test (**B, D, G, I, K, L**).

Figure 4. DNMT3A deficiency facilitates Polθ - mediated TMEJ and fork restart, but not ssDNA gap filling, in leukemia cells. (**A**) FLT3(ITD) (F), FLT3(ITD);*Dnmt3a*^{KD} (FD) and FLT3(ITD);*Tet2*^{KD} (FT) 32Dcl3 cells were irradiated (2Gy) or not. *Left* – representative immunofluorescent staining of Polθ nuclear foci; *Right* – number of foci/nucleus. (**B**) *Central panel*: A diagram illustrating chromosomal TMEJ-del 23bp and TMEJ-del 39bp assays; *Left and right bar panels*: Mean TMEJ-del 23bp and TMEJ-del 39bp activities, respectively. (**C**) *Left panel*: A diagram illustrating DPC-TMEJ (Str = streptavidin); *Right panels*: Mean % of DPC-TMEJ repair in F, FD and FT 32Dcl3 cells and in Lin^{-} mBMCs from *Flt3*$^{ITD/ITD}$ (F) and *Flt3*$^{ITD+/-}$*;Dnmt3a*$^{R882H/+}$ (FD) mBMCs. (**D**) *Left panel:* Schematic diagram of replication fork restart. *Middle panel*: Representative DNA fibers from F, FD, and FT 32Dcl3 cells incubated with or without 12.5 μM ART558. *Right panel:* Mean DNA fiber lengths presented as IdU/CldU length ratio from ≥100 DNA fibers. (**E**) *Left panel:* Schematic representation of S1 nuclease treatment to quantify IdU track length. *Right panel:* Mean IdU track length from ≥100 DNA fibers from each F, FD and FT 32Dcl3 cells. Error bars represent the SD; p values were determined using one-way Anova (**A**, **C**-32Dcl3 panel) and Student's t test (**B, C**-mBMCs panel, **D, E**).

Figure 5. DNMT3A deficiency limited DNA end-resection in leukemia cells. (**A**) The model of DSB end resection favoring TMEJ or HR. (**B-H**) FLT3(ITD) (F), FLT3(ITD);*Dnmt3a*^{KD} (FD) and FLT3(ITD);*Tet2*^{KD} (FT) 32Dcl3 cells were irradiated (2Gy) and incubated for 2 hrs. (**B**) A scheme of BrdU/PCNA assay. (**C**) *Left panel* - Representative immunofluorescence BrdU and PCNA immunostaining are shown. *Middle and right panels* - mean number of BrdU foci and mean BrdU intensity, respectively, per PCNA-positive nucleus. (**D**) A scheme of SMART assay. (**E**) *Left panel* - representative CldU tracks were shown. *Right panel*: mean of DNA fibers length presented as the CIdU track length. (**F**) *Left panel* - representative RPA32 foci detected by immunofluorescence. *Upper right panel* - mean number of RPA32 foci/nucleus. *Lower right panel* - representative Western blots of the nuclear cell lysates detecting RPA14, RPA32 and RPA70; histone 3 (H3) was a loading control. (**G**) *Left panel* – representative RAD51 foci detected by immunofluorescence. *Upper right panel* - mean number of RAD51 foci/nucleus.

Lower right panel – representative Western blots of the nuclear cell lysates detecting RAD51; histone 3 (H3) was a loading control. (**H**) Neutral comet assay; mean % of DNA in the tail. Error bars represent the SD; p values were determined using one-way Anova.

Figure 6. DNMT3A deficiency inhibited PARP1-SMARCAD1-MSH2/MSH3 repressive pathway to facilitate the recruitment of Polθ to DNA. (**A**) FLT3(ITD) (F) and FLT3(ITD);*Dnmt3a*^{KD} (FD) 32Dcl3 cells were irradiated (2Gy) and incubated for 2 hrs. before the analyses. *Left panel* – representative Western blots detecting indicated proteins in total cell lysates and chromatin fractions. Actin and histone H3 served as loading controls. *Right panel* - mean of the indicated protein band intensity. (**B-D**) Lin$^-$ *Flt3*$^{ITD+/+}$ (F) and Lin$^-$ *Flt3*$^{ITD+/+}$*;Parp1*$^{-/-}$ (FP) mBMCs were irradiated (2 Gy) 2 hrs. before the analyses. (**B**) SMART assay. *Left panel* - representative CldU tracks were shown. *Right panel* - mean of DNA fibers length presented as the CIdU track length. (**C**) *Left panels* – representative Western blots detecting indicated proteins in total cell lysates and chromatin fractions. Actin and histone H3 served as loading controls. *Right panels* - mean of the indicated protein band intensity in the chromatin fractions. (**D**) *Left panels* – representative SMARCAD1 and/or γH2AX foci; *Right panels* – mean numbers of co-localizing foci/nucleus. (**E-I**) F and FD 32Dcl3 cells were irradiated (2 Gy) 2 hrs. before the analyses. (**E, G-I**) *Left panels* – representative nuclear foci. *Right panels* – mean numbers of co-localizing foci/nucleus. (**F**) *Left panel* – representative Western blots detecting indicated proteins in total cell lysates and chromatin fractions. Actin and histone H3 served as loading controls. *Right panels* - mean band intensity of the indicated protein in the chromatin fractions. (**J**) F 32Dcl3 cells were transfected with the *Msh2* shRNA (F shRNA Msh2) or Scrambled (F Scr). *Left panel* - Western blot showing downregulation of MSH2 in the former cells; *Middle panel* – representative Polθ nuclear foci; *Right panel* – mean numbers of foci/nucleus. (**K**) SMART assay. *Left panels* - representative CldU tracks were shown. *Right panels* - mean length of DNA fibers presented as the CIdU track length. (**L**) A diagram illustrating how *DNMT3Amut* restrains DSB end resection by inhibiting PARP1-dependent repressive role of SMARCAD1-MSH2/MSH3 complex in the recruitment of Polθ to a DSB. Error bars represent the SD; p values were determined using Student's t test.

Figure 7. Polθi enhanced the sensitivity of DNMT3A deficient leukemia cells to standard drugs. (**A-D**) Sensitivity of FLT3(ITD);*Dnmt3a*^{KD} 32Dcl3 cells (32D), FLT3(ITD);DNMT3A(R882H) Lin$^-$CD34$^+$ AML primary (AML) cells and Lin$^-$CD34$^+$ normal bone marrow cells (NBMCs) to Polθi (25 μM ART558, 50μM ART812, 4μM RP-6685) +/- (**A**) 2.5 nM quizartinib, (**B**) 60 nM etoposide, (**C**) 0.2 μM cytarabine, and (**D**) 0.25μM azacytidine. Results represent mean number of colonies. (**E, F**) FLT3(ITD);*Dnmt3a*^{KD} 32Dcl3 cells (32D) were untreated, or treated with 4 μM RP-6685 and/or 60nM etoposide. (**E**) Mean number of DPCs. (**F**) Mean % of DNA in the tail. (**G**) A scheme of *in vivo* experiments. (**H**) Mean number of GFP$^+$ FLT3(ITD);*Dnmt3a*^{KD} 32Dcl3 cells (FD cells) in PBL of SCID mice untreated (Control) and treated with RP-6685, etoposide (ETO) and the combination (RP-6685+ETO). (**I**) Survival curves and MST of the mice. Error bars represent the SD; p values were calculated using one-way Anova (**A-F, H**); mice survival was evaluated by Kaplan-Meier LogRank test.

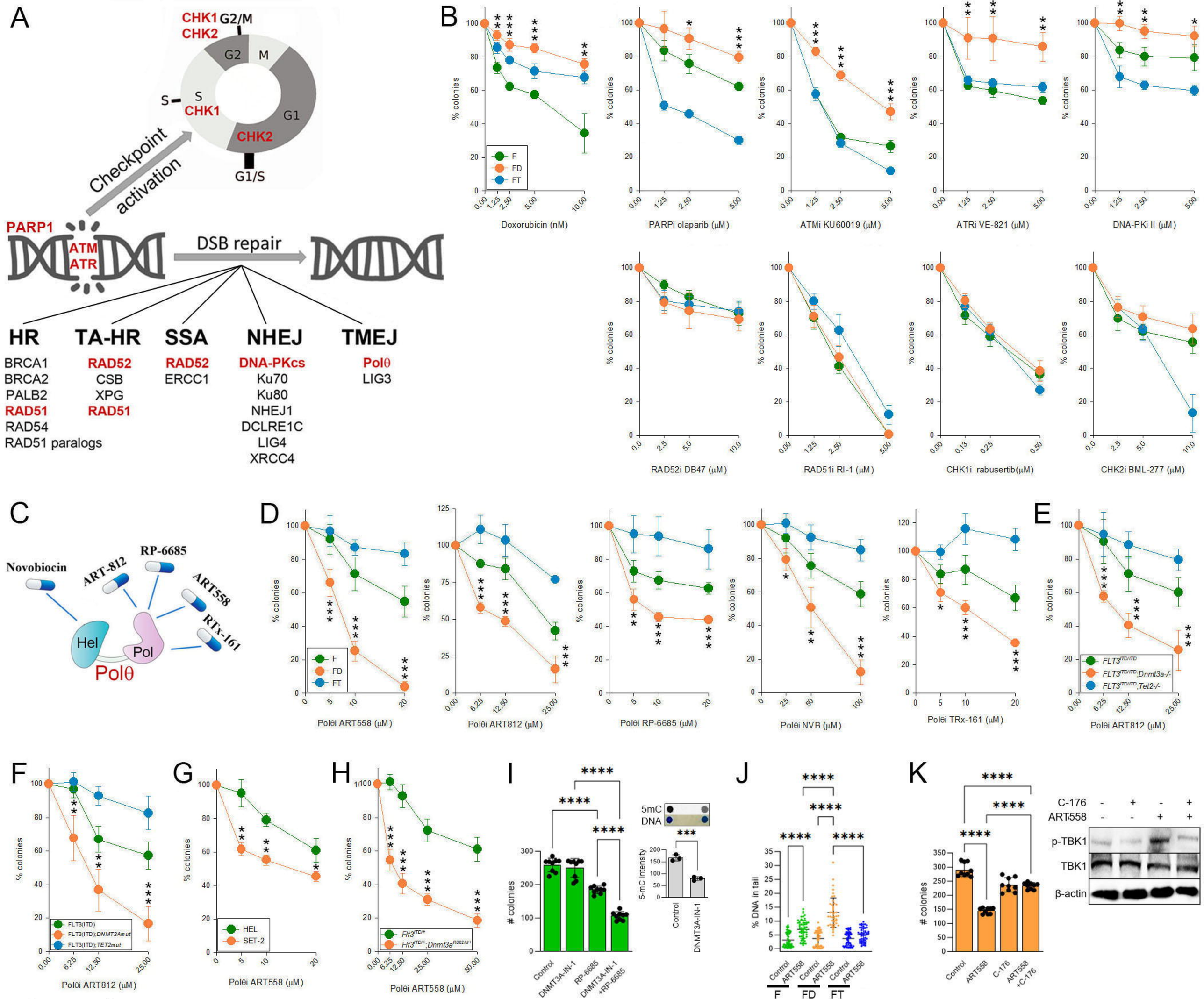
A
CHK1 G2/M
CHK2
G2
M
S
S
CHK1
G1
CHK2
G1/S
Checkpoint activation
PARP1
ATM
ATR
DSB repair
HR
TA-HR
SSA
NHEJ
TMEJ
BRCA1
BRCA2
PALB2
RAD51
RAD54
RAD51 paralogs
RAD52
CSB
XPG
RAD51
RAD52
ERCC1
DNA-PKcs
Ku70
Ku80
NHEJ1
DCLRE1C
LIG4
XRCC4
Polθ
LIG3
B
% colonies
F
FD
FT
Doxorubicin (nM)
PARPi olaparib (μM)
ATMi KU60019 (μM)
ATRi VE-821 (μM)
DNA-PKi II (μM)
RAD52i DB47 (μM)
RAD51i RI-1 (μM)
CHK1i rabusertib(μM)
CHK2i BML-277 (μM)
C
Novobiocin
ART-812
RP-6685
ART558
RTx-161
Hel
Pol
Polθ
D
Polθi ART558 (μM)
Polθi ART812 (μM)
Polθi RP-6685 (μM)
Polθi NVB (μM)
Polθi TRx-161 (μM)
E
FLT3ITD/ITD
FLT3ITD/ITD;Dnmt3a-/-
FLT3ITD/ITD;Tet2-/-
Polθi ART812 (μM)
F
FLT3(ITD)
FLT3(ITD);DNMT3Amut
FLT3(ITD);TET2mut
Polθi ART812 (μM)
G
HEL
SET-2
Polθi ART558 (μM)
H
Flt3ITD/+
Flt3ITD/+;Dnmt3aR882H/+
Polθi ART558 (μM)
I
colonies
Control
DNMT3A-IN-1
RP-6685
DNMT3A-IN-1 +RP-6685
5mC
DNA
5-mC intensity
Control
DNMT3A-IN-1
J
% DNA in tail
Control
ART558
F
FD
FT
K
colonies
Control
ART558
C-176
ART558 +C-176
C-176
ART558
p-TBK1
TBK1
β-actin

Figure 1

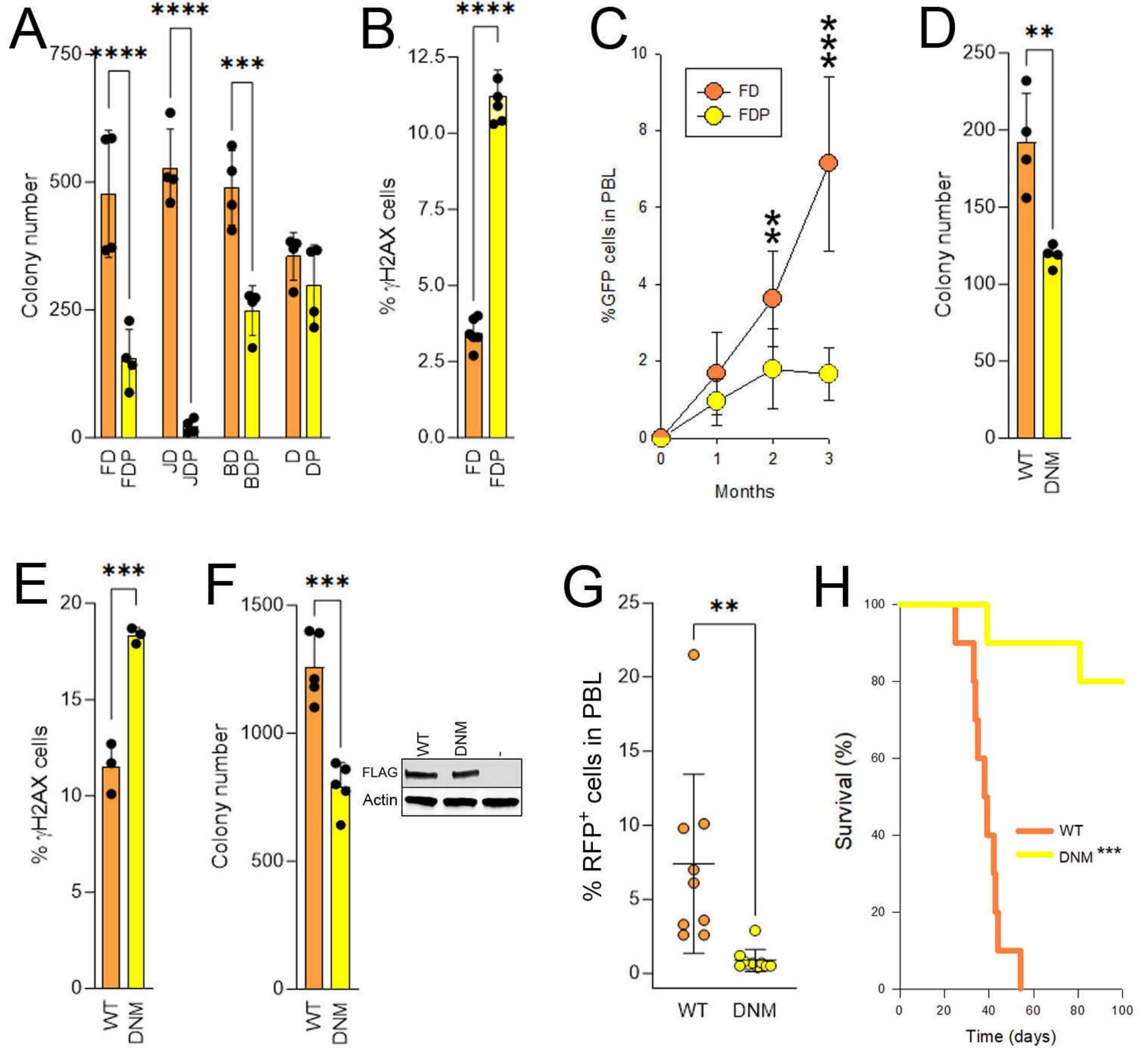
A
Colony number
750
500
250
0
****
****
***
FD
FDP
JD
JDP
BD
BDP
D
DP
B
% γH2AX cells
12.5
10.0
7.5
5.0
2.5
0.0
****
FD
FDP
C
%GFP cells in PBL
10
8
6
4
2
0
FD
FDP
**
***
0
1
2
3
Months
D
Colony number
250
200
150
100
50
0
**
WT
DNM
E
% γH2AX cells
20
15
10
5
0
***
WT
DNM
F
Colony number
1500
1000
500
0
***
WT
DNM
FLAG
Actin
G
% RFP+ cells in PBL
25
20
15
10
5
0
**
WT
DNM
H
Survival (%)
100
80
60
40
20
0
WT
DNM ***
0
20
40
60
80
100
Time (days)

Figure 2.

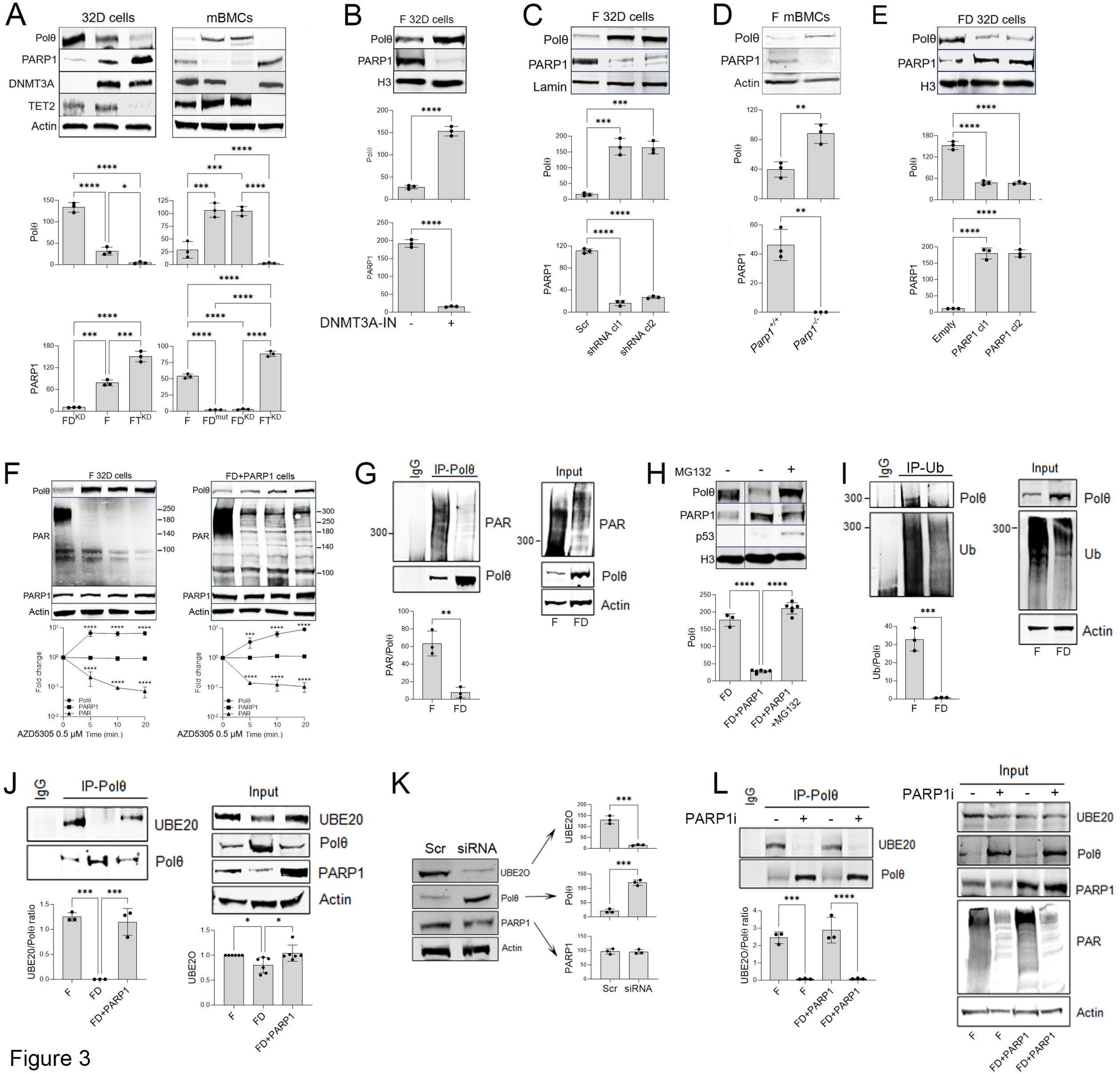
A
32D cells
mBMCs
Polθ
PARP1
DNMT3A
TET2
Actin
FD^KD
F
FT^KD
FD^mut
B
F 32D cells
H3
DNMT3A-IN
C
F 32D cells
Lamin
Scr
shRNA cl1
shRNA cl2
D
F mBMCs
Parp1+/+
Parp1-/-
E
FD 32D cells
Empty
PARP1 cl1
PARP1 cl2
F
F 32D cells
FD+PARP1 cells
PAR
Fold change
AZD5305 0.5 μM Time (min.)
G
IgG
IP-Polθ
Input
PAR/Polθ
H
MG132
p53
FD
FD+PARP1
FD+PARP1 +MG132
I
IP-Ub
Ub
Ub/Polθ
J
UBE20
UBE20/Polθ ratio
UBE2O
K
Scr
siRNA
L
PARP1i

Figure 3

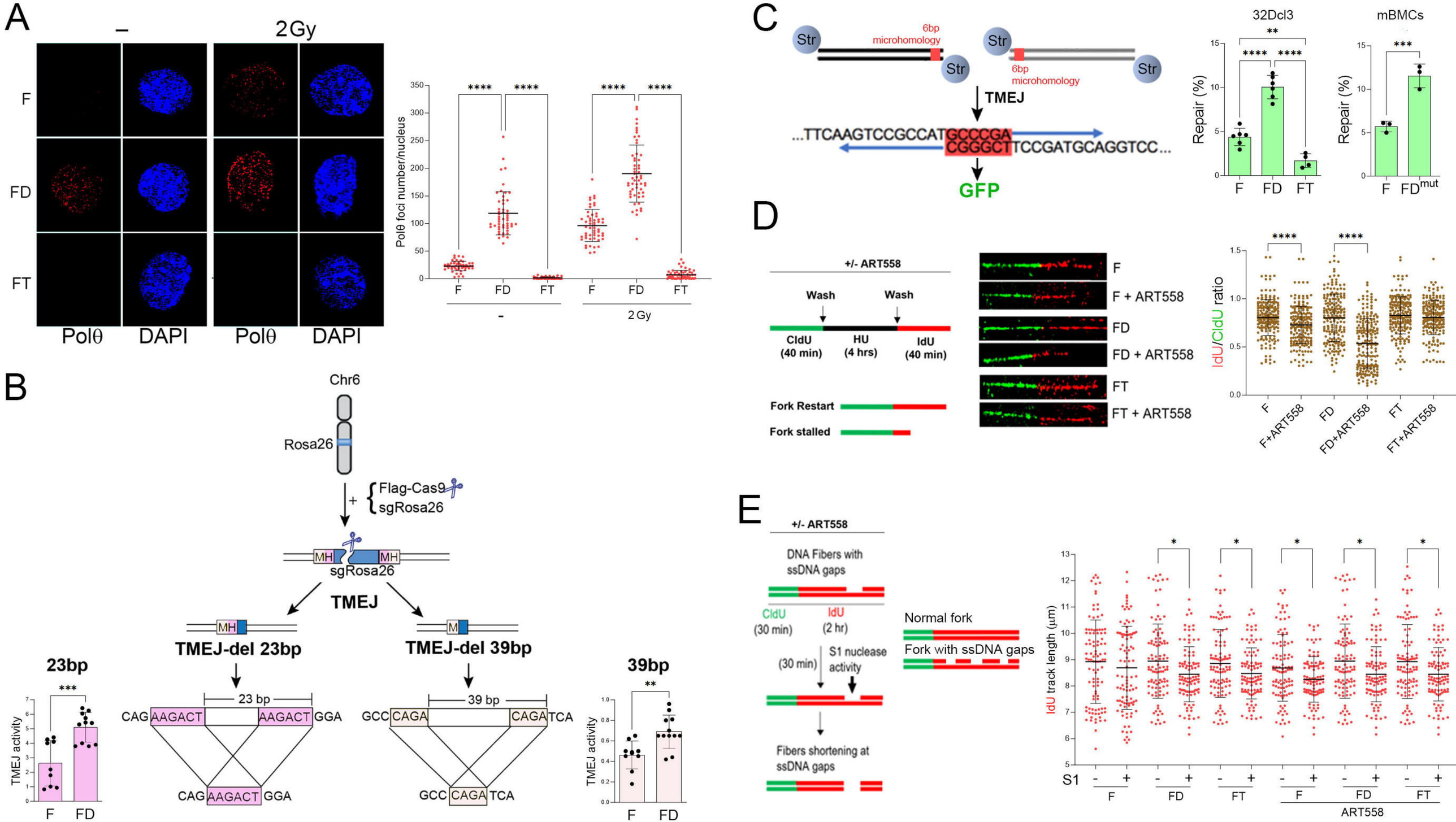
A
–
2Gy
F
FD
FT
Polθ
DAPI
Polθ
DAPI
Polθ foci number/nucleus
****
****
****
****
F
FD
FT
F
FD
FT
-
2Gy
C
Str
6bp microhomology
Str
Str
6bp microhomology
Str
TMEJ
...TTCAAGTCCGCCATGCCCGA
CGGGCTTCCGATGCAGGTCC...
GFP
32Dcl3
mBMCs
Repair (%)
**
****
****
***
F
FD
FT
F
FD^mut
D
+/- ART558
Wash
Wash
CldU (40 min)
HU (4 hrs)
IdU (40 min)
Fork Restart
Fork stalled
F
F + ART558
FD
FD + ART558
FT
FT + ART558
IdU/CldU ratio
****
****
F
F+ART558
FD
FD+ART558
FT
FT+ART558
E
+/- ART558
DNA Fibers with ssDNA gaps
CldU (30 min)
IdU (2 hr)
(30 min)
S1 nuclease activity
Fibers shortening at ssDNA gaps
Normal fork
Fork with ssDNA gaps
IdU track length (µm)
S1
F
FD
FT
F
FD
FT
ART558
B
Chr6
Rosa26
Flag-Cas9
sgRosa26
MH
MH
sgRosa26
TMEJ
MH
M
TMEJ-del 23bp
TMEJ-del 39bp
23 bp
39 bp
CAG AAGACT AAGACT GGA
CAG AAGACT GGA
GCC CAGA CAGA TCA
GCC CAGA TCA
23bp
39bp
TMEJ activity
***
**
F
FD

Figure 4

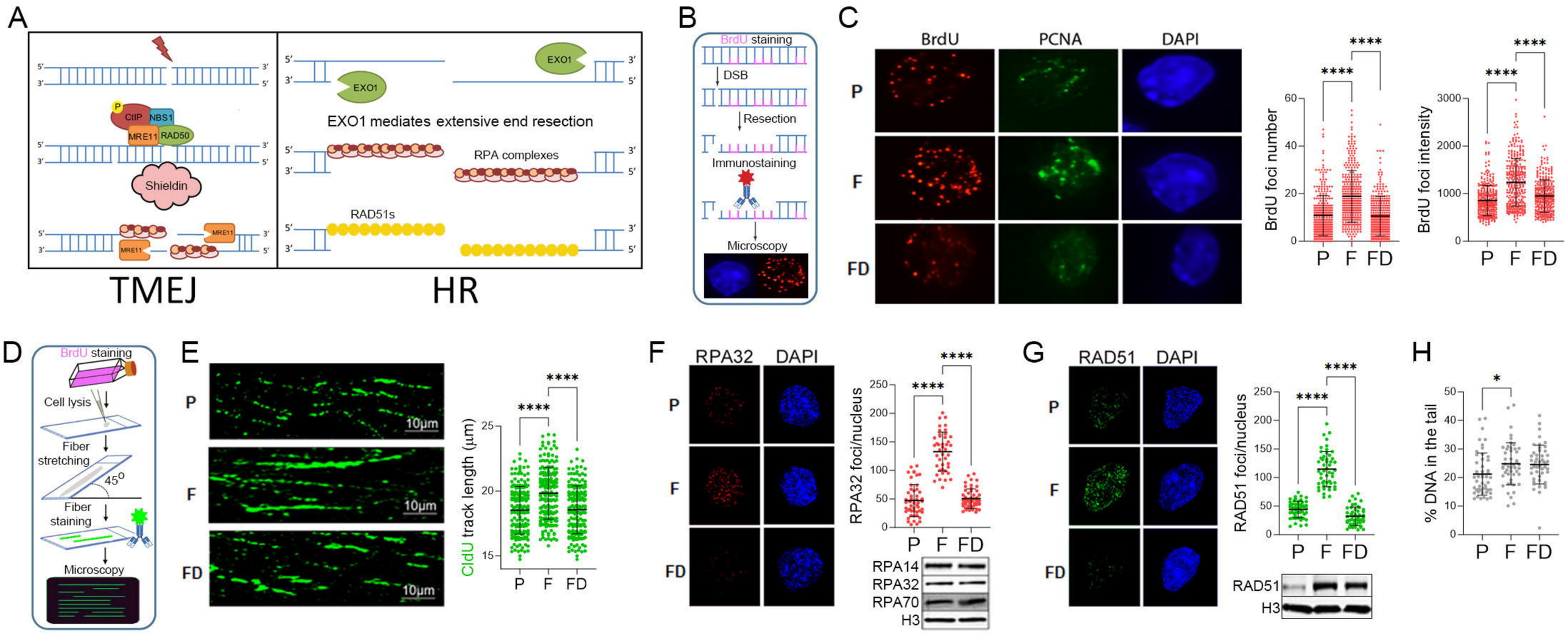
A
5′
3′
P
CtIP
NBS1
MRE11
RAD50
Shieldin
MRE11
EXO1
EXO1 mediates extensive end resection
RPA complexes
RAD51s
TMEJ
HR
B
BrdU staining
DSB
Resection
Immunostaining
Microscopy
C
BrdU
PCNA
DAPI
P
F
FD
BrdU foci number
BrdU foci intensity
****
D
BrdU staining
Cell lysis
Fiber stretching
45°
Fiber staining
Microscopy
E
10μm
CldU track length (μm)
F
RPA32
DAPI
RPA32 foci/nucleus
RPA14
RPA32
RPA70
H3
G
RAD51
DAPI
RAD51 foci/nucleus
RAD51
H3
H
% DNA in the tail
*

Figure 5

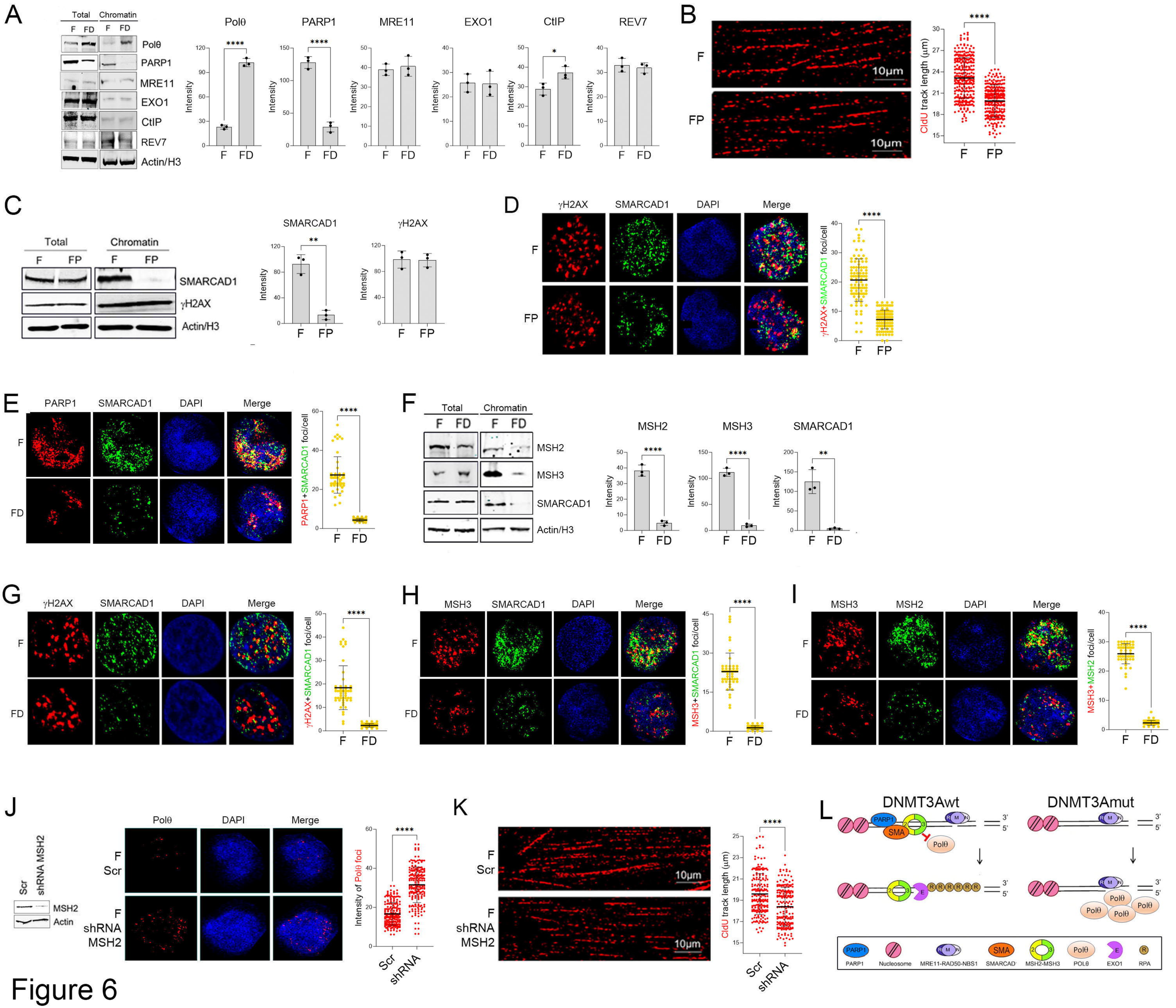
A
Total
Chromatin
F
FD
Polθ
PARP1
MRE11
EXO1
CtIP
REV7
Actin/H3
Intensity
****
*
B
F
FP
10μm
CldU track length (μm)
C
SMARCAD1
γH2AX
**
D
DAPI
Merge
γH2AX+SMARCAD1 foci/cell
E
PARP1+SMARCAD1 foci/cell
F
MSH2
MSH3
G
H
MSH3+SMARCAD1 foci/cell
I
MSH3+MSH2 foci/cell
J
Scr
shRNA MSH2
shRNA
Intensity of Polθ foci
K
L
DNMT3Awt
DNMT3Amut
SMA
3'
5'
PARP1
Nucleosome
MRE11-RAD50-NBS1
SMARCAD
MSH2-MSH3
POLθ
EXO1
RPA

Figure 6

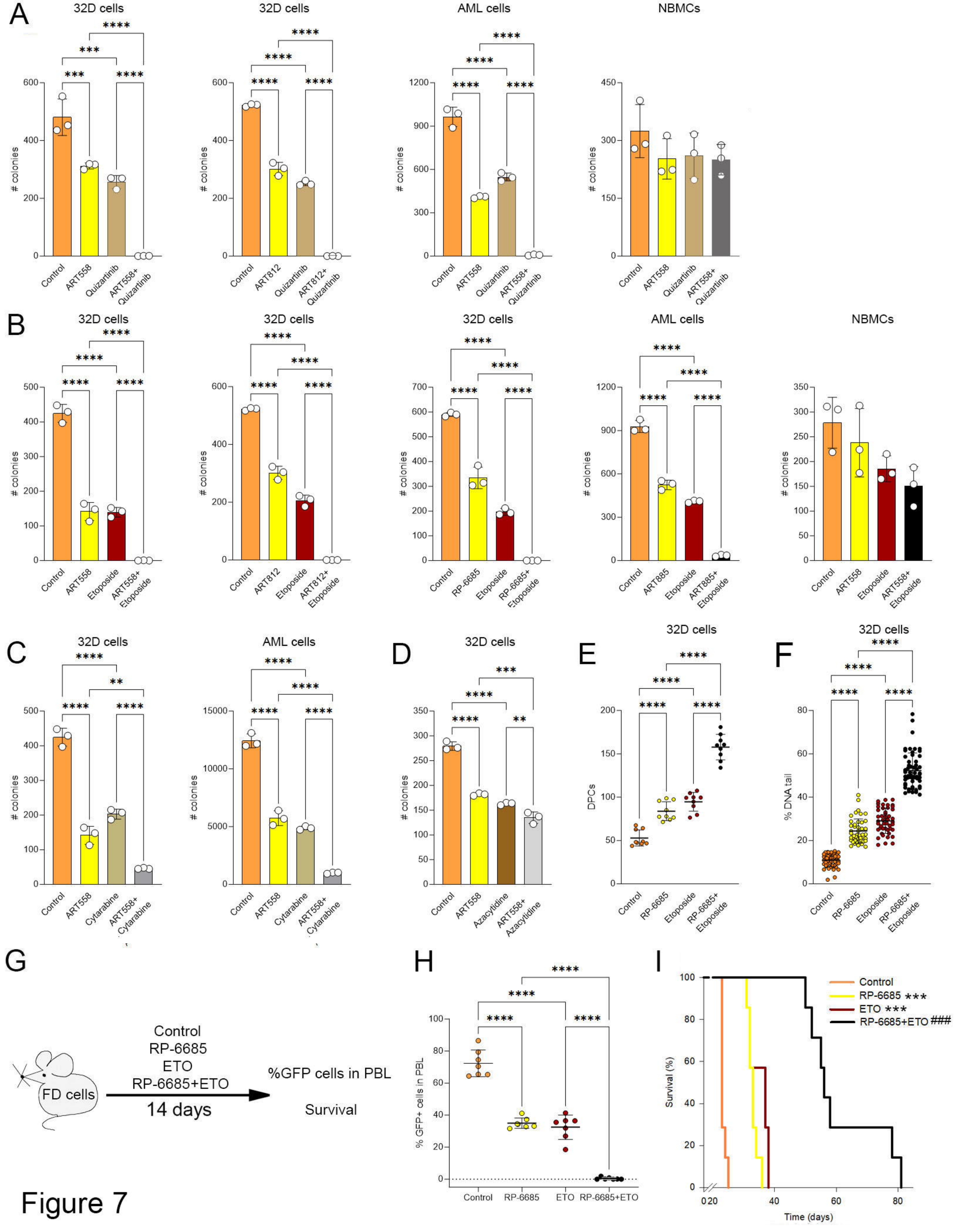
A
32D cells
32D cells
AML cells
NBMCs
colonies
Control
ART558
Quizartinib
ART558+ Quizartinib
ART812
ART812+ Quizartinib
B
Etoposide
ART558+ Etoposide
ART812+ Etoposide
RP-6685
RP-6685+ Etoposide
ART885
ART885+ Etoposide
C
Cytarabine
ART558+ Cytarabine
D
Azacytidine
ART558+ Azacytidine
E
DPCs
RP-6685+ Etoposide
F
% DNA tail
G
FD cells
Control
RP-6685
ETO
RP-6685+ETO
14 days
%GFP cells in PBL
Survival
H
% GFP+ cells in PBL
I
Survival (%)
Time (days)
RP-6685 ***
ETO ***
RP-6685+ETO ###

Figure 7

STAR* METHOD

	SOURCE	IDENTIFIER	RRID
Antibodies			
Anti-RAD51	Santa Cruz	Cat#sc-53428	AB_630180
Anti-Actin	Invitrogen	Cat#:MA5-11869	AB_11004139
Anti-PARP1	Santa Cruz Biotechnology	Cat#:SC-74440	AB_1128605
Anti-POLθ	MyBioSource	Cat#:MBS9612322	Not available
IRDye 800CW	LI-COR	Cat#:926-32210	AB_621842
IRDye 680CW	LI-COR	Cat#:926-68073	AB_10954442
Anti-MRE11	Santa Cruz Biotechnology	Cat#:SC-135992	AB_2145244
Anti-EXO1	Santa Cruz Biotechnology	Cat#:SC-56092	AB_783300
Anti-CtIP	Bethyl Technology	Cat#:A300-488A-T	AB_2632119
Anti-REV7	MyBioSource	Cat#MBS4752863	Not available
Anti-DNA2	Proteintech	Cat#50559521	Not available
Anti-Histone H3	Invitrogen	Cat#PA5-16183	AB_10985434
Anti-MSH2	Invitrogen	Cat#33-7900	AB_2533139
Anti-MSH3	Invitrogen	Cat#PA5-114764	AB_2899400
Anti-H3(R26Cit)	Abcam	Cat#Ab212082	Not available
Anti-RHNO1	Boster	Cat#A13755	Not available
Anti-γH2AX	Abcam	Cat#ab243906	Not available
Anti-SMARCAD1	Abcam	Cat#Ab67548	AB_1142946
Anti-PARP1	Abcam	Cat#Ab194586	AB_2895023
Anti-POLθ	Biorbyt	Cat#orb385434	Not available
Anti-PARG	Invitrogen	Cat#PA5-76538	AB_2720265
Anti-Histone H3	Invitrogen	Cat#AHO-1432	AB_10375008
Anti-Lamin	Abcam	Cat#Ab-16048	AB_443298
Anti-β-Actin	Santa Cruz	Cat#sc-47778	AB_626632
Anti-RPA14	Santa Cruz	Cat#sc-271564	AB_10649042
Anti-RPA32	Abcam	Cat#Ab76420	AB_1524336
Anti-RPA70	Invitrogen	Cat#MA5-36226	AB_2884060
Anti-ALDH2	Invitrogen	Cat#MA5-17029	AB_2538501
Anti-ADH5	Abcam	Cat#Ab177932	Not available
Anti-TDP1	Invitrogen	Cat#PA5-98189	AB_2812803
Anti-TDP2	ProteinTech	Cat#12203 I-AP	AB_1607504
Anti-SPRTN	Bioss	Cat#bs-15013R	Not available
Anti-PLK1	Invitrogen	Cat#37-7100	AB_2533336
Anti-p53	Santa Cruz	Cat#sc-99	AB_628086
Anti-p(Ser172)TBK1	CellSignaling	Cat#5483	AB_10693472
Anti-TBK1	CellSignaling	Cat#3504	AB_2255663
Anti-CtIP	Invitrogen	Cat#PA5-20963	AB_11153016
Anti-UBE2O	Fortis	Cat#A301-873-A	AB_1309799
Anti- γH2AX	MilliporeSigma	Cat# 05-636	AB_309864
Anti-5mC	CellSignaling	Cat#28692	AB_2798962
Anti-UBE2O	Bethyl	Cat#A301-873A	AB_1309799
Anti-HUWE1	ProteinTech	Cat#19430-1-AP	AB_2878579
Anti-TRIP12	GeneTex	Cat#GTX32138	Not available
Anti-WWP2	ProteinTech	Cat#12197-1-AP	AB_10597536

Anti-CHFR	ProteinTech	Cat#12169-1-AP	AB_2080821
Anti-p(Tyr204)ERK1/2	CellSignaling	Cat#5726S	AB_2797617
Anti-ERK1/2	CellSignaling	Cat#4695T	AB_390779
Anti-PAR	MilliporeSigma	Cat#MABC547	AB_2861394
Anti- IdU	BD Biosciences	Cat#347580	AB_10015219
Anti-CldU	Abcam	Cat#ab213715	Not available
Anti-BrdU	Abcam	Cat#ab6326	AB_2313786
Anti-DNMT3A	CellSignaling	Cat#3598	AB_2277449
Anti-TET2	CellSignaling	Cat#45010	AB_2799277
Anti-Mouse Alexa Fluor 594	Life technologies	Cat#A11062	AB_2534109
Anti-Rat Alexa Fluor 488	Life technologies	Cat#A21470	AB_10561519
Anti-Mouse Alexa Fluor 488	Invitrogen	Cat#A11001	AB_2534069
Anti-Rabbit Alexa Fluor 647	Invitrogen	Cat#A21245	AB_2535813
Anti-Rabbit HRP-conjugated	EMD Millipore	Cat#12-348	AB_390191
Anti-Mouse HRP-conjugated	EMD Millipore	Cat#12-349	AB_390192
Anti-BrdU	Cytiva	Cat#RPN202	AB_2314032
Anti-PCNA	Novus	Cat#NBP2-67390	Not available
Anti-Mouse Alexa Fluor 568	Invitrogen	Cat#A11004	AB_2534072
Anti-Rabbit Alexa Fluor 488	Invitrogen	Cat#A11008	AB_143165
Plasmids			
pCL-ECO	Addgene	Cat#12371	Addgene_12371
psPAX2	Addgene	Cat#12260	Addgene_12260
pMD2.G	Addgene	Cat#12259	Addgene_12259
pCMMP-MCS-IRES-mRFP	Addgene	Cat#36972	Addgene_36972
pCDH-EF1-FHC-POLQ	Addgene	Cat#64875	Addgene_64875
pCDH-EF1-FHC-POLQ-DY2230AA	Addgene	Cat#64878	
PARP1 mouse shRNA	Origene	Cat#TL509117	Not available
PARP1 mouse ORF	Origene	Cat# MR211449L4	Not available
HUWE1 mouse shRNA	Origene	Cat#TL503398	Not available
MSH2 mouse shRNA	Dharmacon	Cat# V3SM11241-234501644	Not available
UBE2O mouse siRNA	Dharmacon	Cat#L-064151-01-0020, (J-064151-09, J-0654151-10,J-065151-11,J-064151-12)	Not available
Cell Lines			
32D-Parental		https://web.expasy.org/cellosaurus/CVCL_0118	CVCL_0118

32D-FLT3(ITD)		https://web.expasy.org/cellosaurus/CVCL_WG50	CVCL_WG50
HEL 92.1.7		https://web.expasy.org/cellosaurus/CVCL_2481	CVCL_2481
SET-2		https://web.expasy.org/cellosaurus/CVCL_2187	CVCL_2187
A549		https://web.expasy.org/cellosaurus/CVCL_0023	CVCL_0023
HCC15		https://web.expasy.org/cellosaurus/CVCL_2057	CVCL_2057
Commercial Kits			
OxiSelect™ Comet Assay Kit (3-Well Slides)	Cell Biolabs	Cat#STA-351	Not available
Formaldehyde assay kit	Abcam	Cat#Ab196997	Not available
Zymo Research R2052 Direct-zol RNA MiniPrep	Genesee	Cat#11-331	Not available
SuperScript™ IV First-Strand Synthesis System	Invitrogen	Cat#18091050	Not available
TaqMan™ Gene Expression Master Mix	Invitrogen	Cat#4369542	Not available
TaqMan™ Gene Expression Assay (FAM)	Invitrogen	Cat#4331182	Not available
PicoGreen dsDNA Assay Kit	Invitrogen	Cat#P7589	Not available
Acetaldehyde assay kit	Sigma	Cat#MAK321	Not available
NucleoBond Xtra Maxi kit	Macherey-Nagel	Cat#740414.50	Not available
NucleoSpin Tissue, Mini kit for DNA	Macherey-Nagel	Cat#740952.50	Not available
ROS Detection Cell-Based Assay Kit	Cayman Chemical	Cat#601520	Not available
EpiQuick 8-OHdG DNA Damage Quantification Direct Kit	EpigenTek	Cat# P-6003	Not available
Genomic DNA Extraction Kit	Macherey-Nagel	Cat#740952.250	Not available
EZ DNA Methylation-Lightning kit	Zymo Research	Cat#D5030	Not available
Rapid DNA Ligation Kit	Invitrogen	Cat#K1422	Not available
Chromatin Extraction kit	Abcam	Cat#Ab117152	Not available
Bgl*I*/	Invitrogen	Cat#FD0083	Not available
Not*I*/	Invitrogen	Cat#FD0595	Not available
Growth factors			
Mouse SCF	StemCell Tech	Cat#78064.2	Not available
Mouse IL-3	Pepro Tech	Cat#213-13	Not available
Human IL-6	StemCell Tech	Cat#78050.2	Not available
Inhibitors			

ART-558	MedChemExpress	Cat#HY-141520	Not available
ART-812	MedChemExpress	Cat#HY-139289	Not available
Etoposide	Selleckchem	Cat#S1225	Not available
Cytarabine (AraC)	Selleckchem	Cat#S1648	Not available
5-azacytidin	Selleckchem	Cat#S1782	Not available
Quizartinib	Selleckchem	Cat#S1526	Not available
DNMT3A-IN-1	MedChemExpress	Cat#HY-144433	Not available
DY-46-2	MedChemExpress	Cat#HY-151136	Not available
Novobiocin Sodium	Selleckchem	Cat#S2492	Not available
RP-6685	MedChemExpress	Cat#HY-151462	Not available
KU60019	Sigma	Cat#925701-46-8	Not available
VE-821	Sigma	Cat#1232410-49-9	Not available
DNA-PK Inhibitor II	Sigma	Cat#154447-35-5	Not available
RI-1	Selleckchem	Cat#S8077	Not available
Rabusertib	Selleckchem	Cat#S2626	Not available
BML-277	Selleckchem	Cat#S8632	Not available
C-176	Selleckchem	Cat#S6575	Not available
Volasertib	Selleckchem	Cat#S2235	Not available
ERKi (SCH772984)	Selleckchem	Cat#S7101	Not available
MG132	Sigma	Cat#M7449	Not available
AZD5305	Selleckchem	Cat#S9875	Not available
Cycloheximide	Selleckchem	Cat#S7418	Not available
Hydroxyurea	Sigma	Cat#H-8627	Not available
Softwares			
Prism GraphPad 9	Graphpad	https://www.graphpad.com/scientific-software/prism/	SCR_002798
ImageJ	NIH	https://imagej.nih.gov/ij/	SCR_003070
FlowJo		https://www.flowjo.com/solutions/flowjo	SCR_008520